energies

MDPI

Article

Innovative Smart, Autonomous, and Flexible Solar Photovoltaic Cooking Systems with Energy Storage: Design, Experimental Validation, and Socio-Economic Impact

Bilal Zoukarh [1], Mohammed Hmich [1], Abderrafie El Amrani [1], Sara Chadli [1], Rachid Malek [1], Olivier Deblecker [2], Khalil Kassmi [1,3,*] and Najib Bachiri [3]

[1] Team Electronic Materials & Renewable Energy EMRE, Laboratory of Electromagnetic, Signal Processing & Renewable Energy LESPRE, Department of Physics, Faculty of Science, Mohamed First University, Oujda 60000, Morocco; ab.elamrani@ump.ac.ma (A.E.A.)
[2] Faculty of Engineering-Electrical Power Engineering Unit, University of Mons, 7000 Mons, Belgium
[3] Association Humain and Environnement of Berkane (AHEB), Berkane 63300, Morocco
* Correspondence: khkassmi@yahoo.fr

Abstract

This work presents the design, modeling, and experimental validation of an innovative, highly autonomous, and economically viable photovoltaic solar cooker, integrating a robust battery storage system. The system combines 1200 Wp photovoltaic panels, a control block with DC/DC power converters and digital control for intelligent energy management, and a thermally insulated heating plate equipped with two resistors. The objective of the system is to reduce dependence on conventional fuels while overcoming the limitations of existing solar cookers, particularly insufficient cooking temperatures, the need for continuous solar orientation, and significant thermal losses. The optimization of thermal insulation using a ceramic fiber and glass wool configuration significantly reduces heat losses and increases the thermal efficiency to 64%, nearly double that of the non-insulated case (34%). This improvement enables cooking temperatures of 100–122 °C, heating element surface temperatures of 185–464 °C, and fast cooking times ranging from 20 to 58 min, depending on the prepared dish. Thermal modeling takes into account sheet metal, strengths, and food. The experimental results show excellent agreement between simulation and measurements (deviation < 5%), and high converter efficiencies (84–97%). The integration of the batteries guarantees an autonomy of 6 to 12 days and a very low depth of discharge (1–3%), allowing continuous cooking even without direct solar radiation. Crucially, the techno-economic analysis confirmed the system's strong market competitiveness. Despite an Initial Investment Cost (CAPEX) of USD 1141.2, the high performance and low operational expenditure lead to a highly favorable Return on Investment (ROI) of only 4.31 years. Compared to existing conventional and solar cookers, the developed system offers superior energy efficiency and optimized cooking times, and demonstrates rapid profitability. This makes it a sustainable, reliable, and energy-efficient home solution, representing a major technological leap for domestic cooking in rural areas.

Keywords: photovoltaic solar cooker; thermal insulation; heating plate; energy balance modeling; Runge–Kutta method; heat transfer; simulation et validation experimental; autonomie; rural energy applications

Academic Editor: Carlo Renno

Received: 8 November 2025
Revised: 4 January 2026
Accepted: 8 January 2026
Published: 14 January 2026

1. Introduction

The energy issue is now a major issue on a global scale, not only because of the continuous increase in demand, but also because of the environmental impacts linked to the use of fossil fuels and biomass [1–5]. In the specific field of cooking, this problem takes on a particular dimension, especially in rural areas where access to modern energy remains limited [6–8]. The majority of households still use wood, charcoal or butane gas, the intensive use of which leads to several harmful consequences: accelerated deforestation, depletion of forest resources, and degradation of ecosystems, as well as increased emissions of greenhouse gases and air pollutants. In addition, there are concerning health effects linked to the inhalation of smoke in enclosed spaces, aggravating public health problems [9].

In light of these observations, the development of sustainable, clean, and accessible alternative solutions for cooking appears to be a necessity. The objective is to reduce energy dependence on conventional fuels such as wood and gas, while proposing efficient devices adapted to domestic use.

In the literature, two main types of solar cookers can be distinguished:

- Thermal solar cookers, which directly exploit the heat of solar radiation;
- Electric solar cookers, which use photovoltaic energy to power a heating element.

Thermal solar cookers are available in several configurations:

❖ Parabolic solar cooker: This type concentrates solar rays at a focal point where a cooking vessel is placed. It allows rapid attainment of high temperatures, ensuring fast and efficient cooking, suitable for dishes requiring high thermal intensity. However, this configuration presents several limitations: the need for continuous orientation toward the sun, the large size and weight, limiting portability, difficulty in precise control of the cooking level, and sensitivity to weather conditions. In addition, it is subject to significant thermal losses, reducing its overall efficiency [10–12].

❖ Box-type solar cooker (or insulated solar cooker): This cooker operates by trapping heat inside a closed box, often equipped with a transparent glass cover. The air inside gradually heats up, enabling uniform and gentle cooking suitable for domestic use. This type of cooker is simple and low-cost, but it reaches lower temperatures than parabolic cookers, which increases cooking time, and its efficiency strongly depends on solar irradiance. Portability may also be limited depending on the size and weight of the box [13,14].

❖ Solar oven: This configuration uses reflective surfaces or thermal collectors to concentrate and retain heat around a cooking chamber. It combines insulation and concentration, allowing higher temperatures than box-type cookers and offering better control of the cooking process. However, its manufacturing process is more complex and costly, some models require sun-tracking adjustments, and its performance remains sensitive to variations in solar irradiance, although to a lesser extent than parabolic cookers [15–17].

Despite their effectiveness, thermal solar cookers suffer from significant limitations, including direct dependence on solar irradiance, difficulty in precise temperature control, thermal losses, and portability constraints.

To overcome these limitations, electric solar cookers represent an attractive alternative. These devices rely on a heating element powered by photovoltaic energy, making it possible to generate the heat required for cooking without direct dependence on concentrated solar radiation [18–20]. However, such cookers do not always incorporate an electrical energy storage system or a control unit ensuring optimal regulation according to user needs. Moreover, the lack of thermal insulation around the heating elements leads to substantial heat losses, thereby reducing overall energy efficiency [21].

The integration of effective thermal insulation is therefore essential to limit these losses, improve heat retention at the heating plate, and increase the amount of energy actually available for cooking. The judicious use of insulating materials significantly enhances the thermal behavior of electric solar cookers, making the device more efficient, economical, and better suited to user requirements.

Within this context, the present work focuses on the design, modeling, and realization of a photovoltaic solar cooker with energy storage, developed within the framework of national and international projects [22,23]. The device is intended for both rural and urban areas and meets user requirements in terms of energy availability over the entire daily cycle (day and night), heating power, and cooking temperature.

The system is based on a photovoltaic source coupled with battery storage, enabling continuous operation even under low solar irradiance or in the absence of sunlight. Particular attention has been paid to the integration of high-performance thermal insulation to minimize heat losses and maintain the temperature required for efficient cooking, while optimizing electrical energy consumption. This approach also contributes to improving the overall system efficiency and extending battery lifespan by optimizing the thermal and energetic operating conditions.

To achieve these objectives, the development of a well-insulated electric solar cooker that meets practical requirements, such as efficiency, safety, portability, and cooking control, represents a significant advancement in the field of domestic solar technologies. However, a review of the literature reveals that no study has thoroughly explored the thermal modeling of this type of cooker, which is essential for experimental validation and for predicting its behavior as a function of solar irradiance, available electrical power, and operating conditions.

To address this gap, a rigorous thermal model was developed, incorporating different insulating materials and power supply configurations in order to quantify temperature profile evolution as a function of applied power and food thermal loads. Heat transfer was numerically solved using a one-dimensional fourth-order Runge–Kutta method, providing a reliable estimation of the thermal behavior of the device [24,25]. This approach enables the evaluation of the cooker's energy efficiency, enables the identification of an optimal compromise between technical feasibility and thermal resistance of heating elements, and provides a solid basis for experimental optimization and overall performance improvement, ensuring stable, efficient, economical, and sustainable operation.

In parallel with the modeling phase, a digital monitoring platform was developed to facilitate experimental measurements and operational data collection from one or multiple solar cookers. This platform is based on the MQTT (Message Queuing Telemetry Transport) communication protocol and allows simultaneous remote monitoring of several devices, each identified by a specific topic, ensuring individualized, reliable, and scalable supervision. It enables the verification of proper cooker operation, analysis of behavior under real-world conditions, and collection of exploitable data for subsequent analyses.

As part of this study, experimental tests were conducted at the LETSER laboratory, including the preparation of various dishes under controlled conditions. The measured quantities collected via the digital platform were then compared with numerical simulation results, allowing validation of the proposed thermal model and quantitative evaluation of the prototype's performance.

This work is part of applied research projects aimed at developing a photovoltaic solar cooker with integrated energy storage, combining high electrical and thermal performance. Since 2022, research conducted within the LETSER laboratory has been integrated into international programs such as WBI 3.3 and LEAP-RE SoCoNexGen, dedicated to the design and realization of hybrid solar cookers integrating photovoltaic generation and

energy storage. This approach aims to maximize cooker usability, including in the absence of direct sunlight, and to make solar cooking autonomous, reliable, and accessible to African households, in a context where solar potential remains considerable throughout the year.

2. Description of the Photovoltaic Electric Cooker

2.1. Design and Specifications

The prototype of the proposed cooker is shown in Figure 1. It allows cooking via the heating plate powered by the electrical energy produced by the photovoltaic panels during the day and by the solar batteries during periods of little sunlight or night.

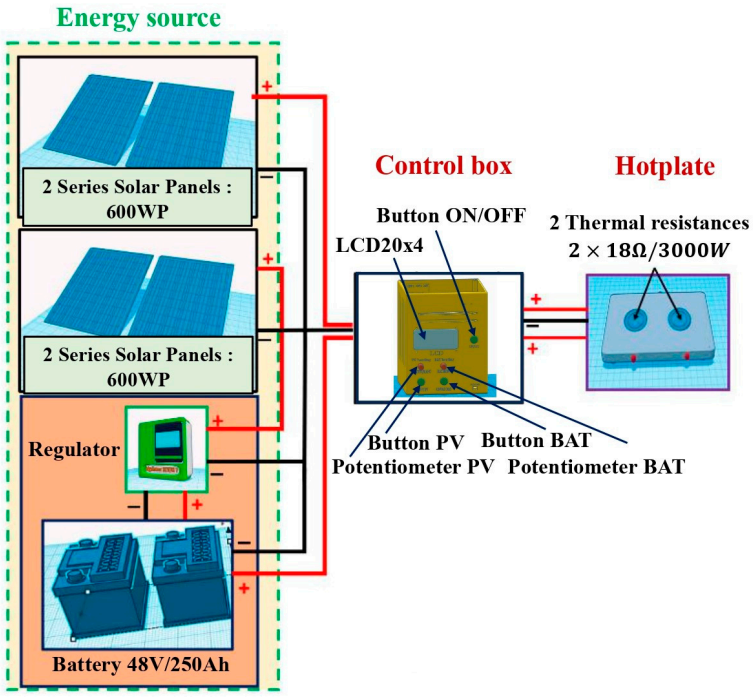

Figure 1. Schematic of the P4 prototype of the photovoltaic solar cooker with dual power supply (direct photovoltaic and 48 V/250 Ah batteries).

The cooker is designed to meet the requirements of the specifications, aimed at providing the energy necessary for cooking over the entire daily cycle (day and night):

- Photovoltaic panels (600 Wp): producing, over 7 h of sunshine, an energy of 3.5 to 4.2 kWh/day, allowing a cooking power of 400 to 450 Wp for 5 h (i.e., 2 to 2.25 kWh/day). The photovoltaic panels, used in our system, are made of high-efficiency polycrystalline cells. The polycrystalline modules were chosen due to their more affordable cost and their performance suited to the sunny regions in question. Each module delivers a nominal power of 300 W, with a maximum power voltage of approximately 35 V and a maximum current close to 8 A under standard irradiation conditions (1000 W/m^2, 25 °C). These modules are interconnected to form a photovoltaic array capable of supplying directly to a DC/DC converter 1 of the electric solar cooker, thus ensuring sufficient power for cooking.
- Batteries (48 V/250 Ah/12 kWh): charged by two additional PV panels (600 Wp each, producing 3.5 to 4.2 kWh/day), to ensure cooking at night or on days with little sunlight. The cooking power varies from 200 to 450 W for 5 h (i.e., 1 to 2.25 kWh/day). The batteries provide power during the night and on days with little sunlight, thus guaranteeing continuous cooking, via a DC/DC converter 2. They are recharged by two photovoltaic modules with a total power of 600 Wp, capable of providing between 3.5 and 4.2 kWh per day under an average of 7 h of sunshine, via a charge

controller. This regulator ensures optimal load management, maintaining a stable voltage of 48 V, while protecting the system from overcharging and deep discharging. The stored energy is used to power the griddles according to the needs of the users, with an adjustable cooking power of between 200 and 450 W for 5 h, i.e., a daily energy consumption of 1 to 2.25 kWh. The total capacity of the battery bank, estimated at 12 kWh, therefore offers a cooking autonomy of between 5 and 12 days without solar gain, guaranteeing high reliability and long-term energy independence of the cooking system.

- Total energy available for cooking, combining PV panels and batteries in the range of 3 to 4.5 kWh/day.
- A control box consisting of two main elements:
  - Block 1, or power card (DC/DC converters 1 and 2), responsible for the conversion and management of the energy provided by the photovoltaic panels and batteries.
  - Block 2, or electronic control board, integrating a Raspberry Pi Pico W microcontroller. The latter ensures the overall supervision of the system: power supply from the PV panels and/or batteries, acquisition and display of electrical quantities, and detection of malfunctions, as well as manual or automatic control of the device. This box has a compact and functional structure. Its front panel includes:
    - ✓ One main ON/OFF push button.
    - ✓ Two selection buttons to choose the power source: photovoltaic (PV) or battery.
    - ✓ Two potentiometers to adjust the operation according to the mode chosen.
    - ✓ The first potentiometer, equipped with an integrated switch, allows you to switch between manual PV mode and automatic mode, regulated by the MPPT (Perturb and Observe) algorithm.
    - ✓ The second potentiometer, combined with battery mode, offers the possibility of directly adjusting the duty cycle, thus ensuring precise and modular control of the power supplied to the heating elements, depending on the energy source used.
- The heating plate (Figure 2) is the central element of the photovoltaic solar cooker prototype, ensuring the conversion of the electrical energy provided by the photovoltaic panels or batteries into heat for cooking. It consists of a 1.85 mm thick iron cover sheet offering strength, homogeneous heat distribution, and adapted thermal inertia, containing two independent heating cores, each equipped with a resistance of 18 Ω, one powered by the photovoltaic panels and the other by the batteries, allowing performance to be evaluated separately according to the power supply mode. The plate is 50 cm wide, 32.5 cm deep, and 6 cm high, with the heating cores having a diameter of 19.5 cm and a spacing of 9 cm, all resting on a 4 cm insulating base for a total height of 10 cm. Thermal insulation has been optimized by combining different materials according to their thermophysical properties and local availability: ceramic fiber for its low conductivity and resistance to high temperatures, glass wool for its very low conductivity and lightness, and Bakelite as a complementary insulator in areas with intermediate temperatures. These materials are positioned around and under the plate to limit heat loss through conduction and convection, and the bottom part is protected by a metal cover, ensuring mechanical durability, safety, and efficient heat flow management. The whole constitutes a high-performance thermal barrier, guaranteeing both good energy efficiency and the structural integrity of the solar cooker.

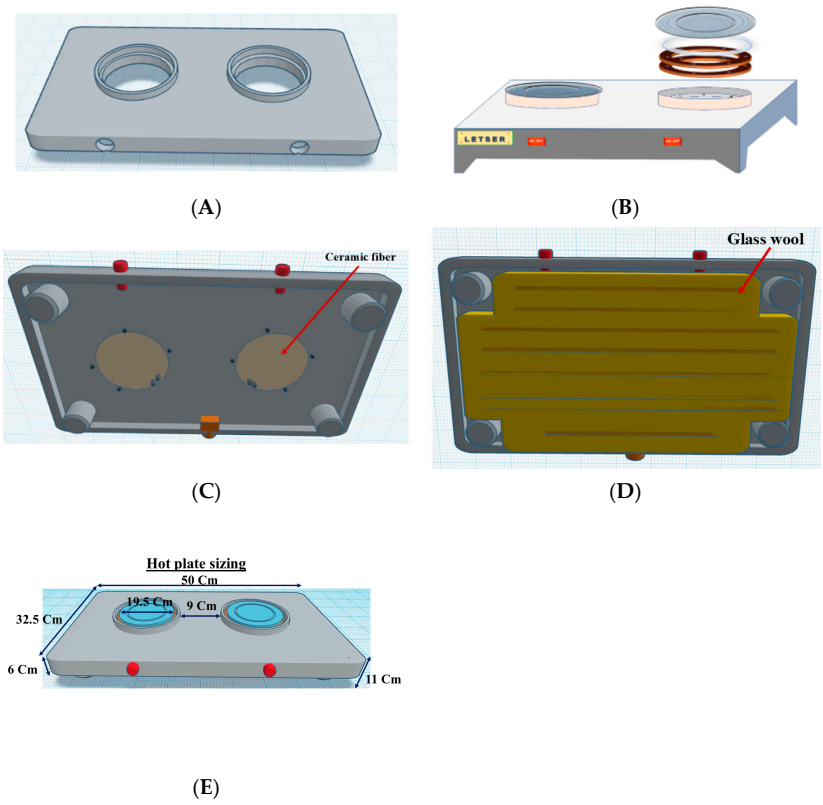

Figure 2. Structure of the heating plate with insulation. (**A**): Metal support of the heating plate. (**B**): Position of the Bakelite rings between the resistor and the sheet metal (front side). (**C**): Ceramic insulation of the resistor (back side). (**D**): Glass wool insulation of the heating plate (back side). (**E**): Final shape of the hot plate.

2.2. Synoptic Diagram and Operating Principle of the Cooker

The synoptic diagram of the photovoltaic solar cooker illustrates all the constituent elements and their interaction: the power sources, the control block, and the heating plate. The detailed architecture and the interaction between these components are shown in Figure 3.

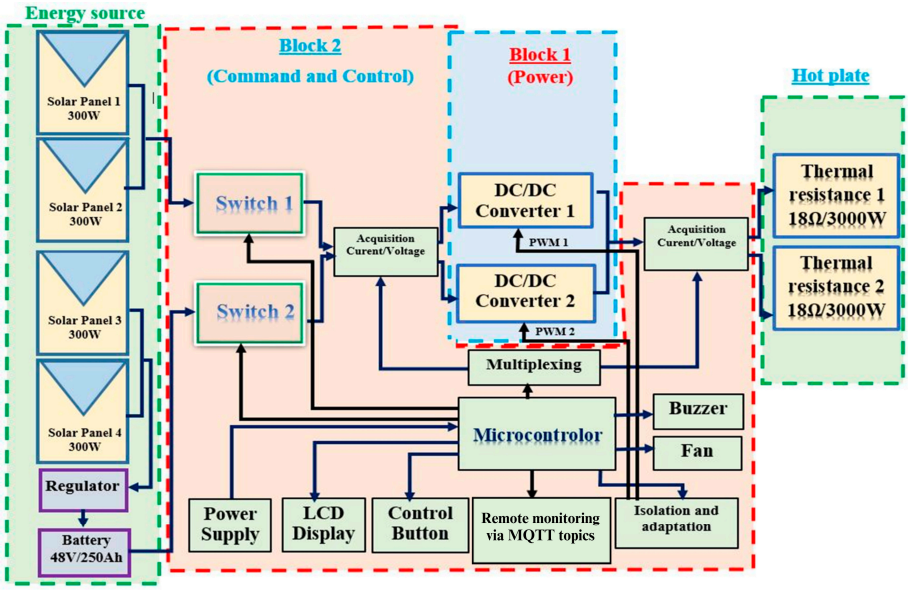

Figure 3. Synoptic diagram of the cooker and the structure of the photovoltaic energy system. (Blocks: 1 and 2).

The control block consists of two main sub-assemblies:

- Block 1 integrates two Boost-type DC/DC converters operating at 20 kHz for a power of 1 kW, the first being powered by the 600 Wp photovoltaic panels in sunny periods, and the second by solar batteries (48 V/250 Ah, four 12 V/250 Ah batteries in series) during periods of low sunlight or night. These batteries, which are recharged by two other 600 Wp PV modules via a charge–discharge controller, also ensure the continuous polarization of the auxiliary circuits (+5 V and +15 V).
- Block 2 brings together the analog and digital circuits distributed on a control board driven by a Raspberry Pi microcontroller and a switch board, including two switches dedicated to the panels and batteries. The microcontroller manages all the functions of the cooker: maximum power point (MPPT) monitoring or manual control of the DC/DC converters via PWM signals with a variable duty cycle, automatic switching between power sources, and real-time acquisition and display of electrical and thermal quantities, as well as detection and protection against anomalies (overvoltage, overcurrent, and disconnection of resistors). To make the most of solar energy, an MPPT algorithm based on the Perturb and Observe method is integrated into the DC/DC converter (Figure 4), allowing the input voltage to be continuously adjusted and converged to the point of maximum power, even in the event of irradiation or temperature variations. This modular and intelligent architecture ensures optimal energy efficiency, precise control of the heating plate, and local or remote supervision suitable for both experimentation and domestic use. The flowchart in Figure 4 illustrates the operation of the Perturb and Observe (P&O) method used to monitor the maximum power point (MPPT) of photovoltaic panels. With each iteration, the system measures the voltage and current of the panels in order to calculate the current power. It then compares this power with that of the previous iteration to determine the variation in power (ΔP) and voltage (ΔV). If the power increases as a result of a disturbance (change in duty cycle D), it means that the system has moved closer to the point of maximum power, and therefore continues to disturb in the same direction. On the other hand, if the power decreases, the direction of the disturbance is reversed. This process repeats continuously, allowing the converter to dynamically adjust the duty cycle to keep the panel operation close to MPP.

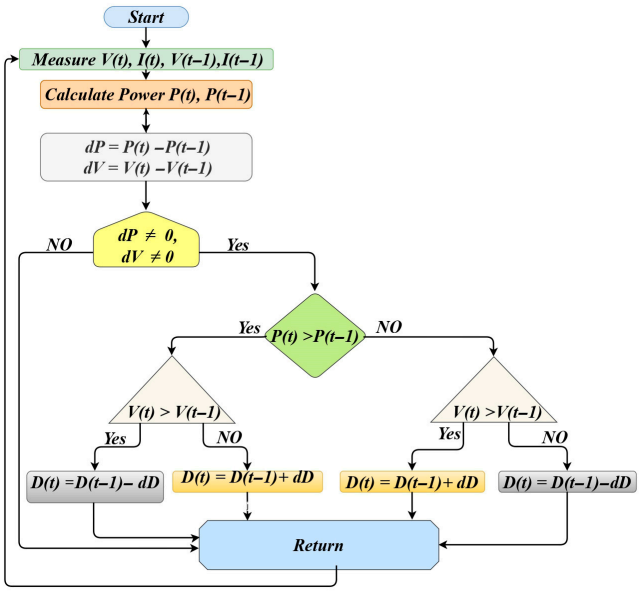

Figure 4. Flowchart of the MPPT Pertub and Observe control used to regulate and optimize the operation of photovoltaic panels over the sun.

3. Thermal Modeling of the Heating Plate

3.1. Modeling Hypothesis

The thermal modeling of the photovoltaic solar cooker is based on a set of simplifying assumptions to describe the thermal behavior of the system while maintaining an acceptable accuracy compared to experimental observations. These hypotheses are justified by the nature of the physical problem studied and by the limitations of the numerical methods used:

- General assumptions: The developed model adopts a one-dimensional (1D) approach to heat transfer. Heat flows are assumed to propagate only in the vertical direction, perpendicular to the surfaces. This simplification is justified by the geometric symmetry of the device and the predominance of vertical transfers over lateral losses. Recognized limitation: this hypothesis neglects lateral heat losses, which can induce a slight discrepancy between the simulated and experimental results, especially at high temperatures. The thermophysical properties of materials (thermal conductivity, specific heat, and density) are considered to be variable with temperature in order to better represent the real behavior of materials subjected to large thermal gradients. This approach improves the accuracy of the thermal model, especially for elements that are highly exposed to solar radiation. Variations in λ(T), Cp(T), and ρ(T) are integrated as empirical relationships or tabulated values from the literature, covering the entire temperature range observed experimentally. Each material in the system (stainless steel, Bakelite, ceramic fiber, glass wool, and silicone) is considered homogeneous and isotropic, with identical properties in all directions. The system is also closed, without mass exchange with the outside, and operates at constant atmospheric pressure (P = 1 atm) for the duration of the simulation.
- Hypotheses on heat transfers: Heat transfers inside the cooker are mainly the result of conduction, natural convection, and radiation phenomena, modeled according to the following principles: perfect thermal contact between the layers, without contact resistance or air gap between the surfaces in contact (resistance–stainless steel, stainless steel–joint, joint–support, and stainless steel–teapot). The natural convection coefficients h_{cv} are calculated from the classical correlations of Nusselt, Grashof, and Prandtl, distinguishing between $h_{cv,b}$ (hot surface facing downwards) and $h_{cv,h}$ (hot surface facing upwards). The properties of air (viscosity, conductivity, and density) vary with temperature in order to ensure an accurate calculation of dimensionless numbers. The surfaces are considered to be gray bodies of constant emissivity. Radiation and convection between the stainless steel plate and the side walls of the glass teapot are neglected. No internal convection is considered in porous insulating materials (glass wool and ceramic fiber); only transfer by effective conduction is taken into account. The entire system is supposed to be perfectly sealed, with no air infiltration between the insulating layers. The temperature is assumed to be uniformly distributed in the volume of water (perfect mixing hypothesis). The influence of the position of the teapot is neglected, with the local effect on the amount of heat captured being considered secondary. Heat exchanges through the mechanical fasteners (hooks, screws, and gluing points) connecting the stainless steel plate to the support are considered negligible.
- Boundary and initial conditions: The ambient temperature is set at T_{amb} = 27 °C and assumed to be constant throughout the simulation. At t = 0, all system temperatures are initialized to the values measured experimentally at the beginning of each test. The power delivered by the battery-panel system is assumed to be constant at 350 W throughout the operating time. Despite these simplifications, the model maintains a high physical consistency and allows obtaining results consistent with experimental

observations, thus providing a solid basis for the simulation and analysis of the thermal performance of the photovoltaic solar cooker.

3.2. Energy Balance and Heat Transfer Equations

The thermal modeling of the photovoltaic solar cooker is based on an energy balance for each major component of the system. These balances take into account the mechanisms of heat transfer: conduction (between adjacent components), natural convection (with ambient air), and radiation (to the environment). The equations are formulated in the form of ordinary differential equations (ODEs) describing the temporal evolution of the temperatures. To generalize the formulation, we present a single equation per component, including all possible terms from the different insulation configurations. Each term is explained above with the corresponding equation. Terms that are not relevant to a given configuration are simply zeroed or omitted during numerical resolution. This allows for a modular approach that can be adapted to the four cases studied:

- Without thermal insulation: Direct transfers without additional insulating materials.
- With Bakelite: Added Bakelite rings for side insulation.
- With Bakelite and Glass Wool: Side Bakelite + glass wool at the bottom for better retention.
- With ceramic fiber and glass wool: Ceramic fiber + glass wool, for optimal high-temperature insulation.

Two sub-configurations are considered for each case: empty (without additional heat load) and with water (1 L of water in a glass teapot, modeling real cooking). ODEs are solved numerically via the RK4 method in Python (version 3.12).

Energy Balance and Thermal Models

The studied cooking system has an energy balance involving three simultaneous heat transfer modes: conduction through solid materials, natural convection at fluid-solid interfaces, and infrared thermal radiation with the environment.

Figure 5 illustrates the geometric configuration of the cooker as well as all the energy flows. The heart of the system consists of an 18 Ω heating element powered by 350 W of electrical power, generating heat by the Joule effect. This thermal energy propagates along three distinct paths:

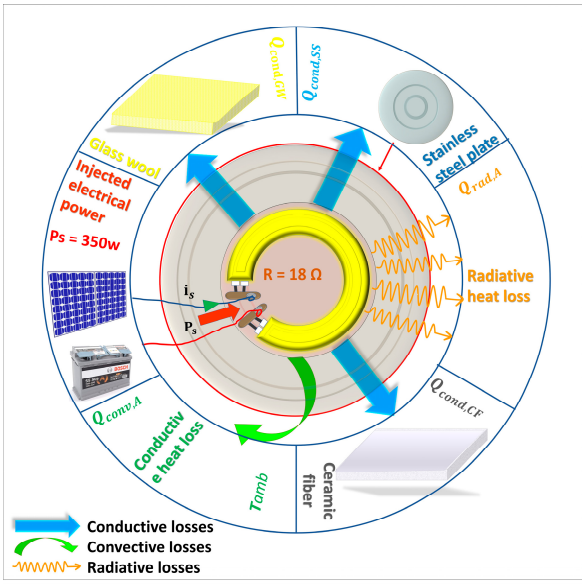

Figure 5. Diagram of heat transfers in the solar cooker.

The conductive transfer, represented by blue arrows, ensures the propagation of heat from the resistor to the cooking vessel through the concentric layers of materials. Convective losses, symbolized by green arrows, occur at the level of the outer surfaces where temperature gradients induce fluid movements. The radiative losses, represented by wavy orange arrows, follow the Stefan–Boltzmann law and depend on the emissivities of the surfaces as well as their absolute temperatures.

To optimize energy efficiency, a multi-layer architecture of thermal insulation limits its heat leakage. Ceramic fiber provides an initial thermal barrier to high-temperature areas, glass wool provides an intermediate layer of insulation, and Bakelite protects the structural support.

On this basis, the energy balance equations for each component are established and presented by the equations with the parameters used given in Appendix A (Table A1):

- Heating element: The heating element (18 Ω) is the central element in the conversion of electrical energy into heat by the Joule effect. Its energy balance is fundamental to understanding the thermal dynamics of the photovoltaic solar cooker. The balance is based on the principle of energy conservation; the variation in the internal energy of the resistor is equal to the difference between the power injected and the outgoing heat fluxes (conduction, convection, and radiation):

$$\frac{dT_r}{dt} = \frac{1}{m_r\, C_{p,r}} \cdot [P_s - Q_{cond,SS} - Q_{cond,r,GW} - Q_{cond,CF} - Q_{conv,A} - Q_{rad,A}]$$

$$\frac{dT_r}{dt} = \frac{1}{m_r\, C_{p,r}} \cdot \left[P_s - \frac{\lambda_{SS}}{L_{SS}} \cdot S_r \cdot (T_r - T_{SS}) - \frac{\lambda_{GW}}{L_{GW}} \cdot S_r \cdot (T_r - T_{GW}) - \frac{\lambda_{CF}}{L_{CF}} \cdot S_r \cdot (T_r - T_{CF}) - h_{cv} . S_r \cdot (T_r - T_{amb}) \right.$$
$$\left. - \sigma \cdot \varepsilon_{eff,r} \cdot S_r \cdot \left((T_r + 273)^4 - (T_c + 273)^4 \right) \right]$$

where

- P_S: The power refers to the electrical power delivered at the output of the solar cooker control box. It is used to directly supply the heating plate, where it is converted into thermal energy through the Joule effect. In this model, (P_s) is assumed to be constant and set to a value of P_s = 350 W.

$$P_s = R \cdot I^2$$

This power is the main energy input of the system and is fully converted into heat.

- $Q_{cond,SS}$: Heat flow transferred by heat conduction between the heating element and the stainless steel plate above. It is a function of the temperatures, the contact surface, the thickness of the plate, and the thermal conductivity of the stainless steel, according to the expression [26]:

$$Q_{cond,SS} = \frac{\lambda_{SS}}{L_{SS}} \cdot S_r \cdot (T_r - T_{SS})$$

- $Q_{cond,r,GW}$: Heat flow transferred by conduction to glass wool. It is a function of temperature, surface area, thickness, and thermal conductivity, according to the expression [26]:

$$Q_{cond,r,GW} = \frac{\lambda_{GW}}{L_{GW}} \cdot S_r \cdot (T_r - T_{GW})$$

- $Q_{cond-fibre}$: Heat flow transferred by conduction to the ceramic fiber. It is a function of the temperatures, the surface, the thickness, and the thermal conductivity, according to the expression:

$$Q_{cond,CF} = \frac{\lambda_{CF}}{L_{CF}} \cdot S_r \cdot (T_r - T_{CF})$$

- $Q_{conv,A}$: Heat losses by natural convection between the surface of the resistor and the ambient air. They are calculated as a function of the two temperatures, the exchange surface, and the natural convection coefficient (W/(m^2 · K)) for a hot surface facing downwards [27,28]:

$$Q_{conv,A} = h_{cv\_b} \cdot S_r \cdot (T_r - T_{amb})$$

where

✓ h_{cv}: Natural convection coefficient for a hot surface facing downwards or upwards (W/m^2 · K). It is determined from the Nusselt number, which itself is a function of the Grashof and Prandtl numbers [29]:

$$h_{cv} = \frac{(Nu)_i \lambda_i}{d_{v,i}}$$

- $Q_{rad,A}$ is the radiant heat flux (W) given by the equation [26,28]:

$$Q_{rad,A} = \sigma \cdot \varepsilon_{eff,r} \cdot S_r \cdot \left(\left(T_r + 273 \right)^4 - \left(T_c + 273 \right)^4 \right)$$

- Stainless steel plate: The stainless steel plate is the cooking surface of the photovoltaic solar cooker. It receives heat from the conductive heating element and redistributes it to the individual components of the system as well as to the cookware (teapot). The heat exchange model of the temperature of the stainless steel plate is written as a function of the temperature of the resistor, the temperatures of the adjacent components (the silicone gasket, insulating material, and teapot), the ambient temperature, the heat flux received by conduction from the resistor, the heat flows transferred by conduction to the gasket, insulation, and teapot, heat losses by natural convection to the ambient air, and losses by thermal radiation to the environment, by the expression:

$$\frac{dT_{SS}}{dt} = \frac{1}{m_{SS} C_{p,SS}} \cdot \left[Q_{cond,SS} - Q_{cond,\mathrm{Ga}} - Q_{cond,\mathrm{SS,B}} - Q_{cond,\mathrm{SS},CF} - Q_{cond,\mathrm{SS,G}} - Q_{conv,\mathrm{SS,A}} - Q_{rad,\mathrm{SS,A}} \right]$$

$$\begin{aligned} \frac{dT_{SS}}{dt} = \frac{1}{m_{SS} C_{p,SS}} \cdot & \left[\frac{\lambda_{SS}}{L_{SS}} \cdot S_r \cdot (T_r - T_{SS}) - \frac{\lambda_{Ga}}{L_{Ga}} \cdot S_{Ga} \cdot (T_{SS} - T_{Ga}) - \frac{\lambda_B}{L_B} \cdot S_{SS,B} \cdot (T_{SS} - T_B) - \frac{\lambda_{CF}}{L_{CF}} \cdot S_{SS,CF} \right. \\ & \cdot (T_{SS} - T_{CF}) - \frac{\lambda_G}{L_G} \cdot S_G \cdot (T_{SS} - T_{SS}) - h_{cv,h} \cdot S_{ss} \cdot (T_{SS} - T_{amb}) - h_{cv,h} \cdot (S_{SS} - S_G) \\ & \left. \cdot (T_{SS} - T_{amb}) \sigma \cdot \varepsilon_{SS} \cdot (S_{SS} - S_G) \cdot \left(\left(T_{SS} + 273 \right)^4 - \left(T_c + 273 \right)^4 \right) \right] \end{aligned}$$

where

- $Q_{cond,\mathrm{Ga}}$: Heat flow exiting by thermal conduction to the high-temperature silicone gasket placed between the stainless steel plate and the support. It is a function of the temperatures, the annular surface of the gasket, the thickness of the gasket, and the thermal conductivity of the silicone [26]:

$$Q_{cond,\mathrm{Ga}} = \frac{\lambda_{Ga}}{L_{Ga}} \cdot S_{Ga} \cdot (T_{SS} - T_{Ga})$$

- $Q_{cond,\mathrm{SS,B}}$: Heat flow transferred by conduction to the Bakelite rings. It depends on the temperatures, the stainless steel-Bakelite contact surface, the thickness of the rings, and the thermal conductivity of the Bakelite [26]:

$$Q_{cond,\mathrm{SS,B}} = \frac{\lambda_B}{L_B} \cdot S_{SS,\mathrm{B}} \cdot (T_{SS} - T_B)$$

- $Q_{cond,\mathrm{SS,CF}}$: Heat flow transferred by conduction to the ceramic fiber disk. It is a function of the temperatures, the contact surface, the thickness of the disk, and the thermal conductivity of the fiber:

$$Q_{cond,\mathrm{SS,CF}} = \frac{\lambda_{CF}}{L_{CF}} \cdot S_{inox\_fibre} \cdot (T_{SS} - T_{CF})$$

- $Q_{cond,\mathrm{SS,G}}$: Useful heat flow transferred by conduction to the cooking utensil (borosilicate glass teapot). It is a function of the temperatures, the contact surface (bottom of the teapot), the thickness of the bottom of the teapot, and the thermal conductivity of the borosilicate glas:

$$Q_{cond,\mathrm{SS,G}} = \frac{\lambda_G}{L_G} \cdot S_G \cdot (T_{SS} - T_{SS})$$

- $Q_{conv,\mathrm{SS,A}}$: Heat losses due to natural convection between the upper surface of the stainless steel plate and the ambient air. They are calculated as a function of the temperatures, the exposed surface, and the natural convection coefficient ($\mathrm{W/(m^2 \cdot K)}$) for an upward-facing hot surface, determined from the Nusselt number:

$$Q_{conv,\mathrm{SS,A}} = h_{cv,h} \cdot (S_{SS} - S_G) \cdot (T_{SS} - T_{amb})$$

- $Q_{rad,\mathrm{SS,A}}$: Heat losses by infrared radiation between the upper surface of the stainless steel plate and the environment according to the Stefan–Boltzmann law. They are calculated according to the absolute temperatures, the surface area, the emissivity of the polished stainless steel, and the Stefan–Boltzmann constant:

$$Q_{rad,\mathrm{SS,A}} = \sigma \cdot \varepsilon_{SS} \cdot (S_{SS} - S_G) \cdot \left(\left(T_{SS} + 273 \right)^4 - \left(T_c + 273 \right)^4 \right)$$

- Conduction seal: The insulating seal receives heat by thermal conduction from the stainless steel plate, and then transmits this heat to the bottom support, also by conduction. This component does not experience convection or radiation, which is consistent with its function as a thermal insulator and its internal position in the system. Its main role is to ensure a limited transfer of heat between two solid masses. The energy balance is based on the principle of energy conservation: the variation in the internal energy of the joint is equal to the difference between the incoming flow (stainless steel) and the outgoing flows (insulating worms or support):

$$\frac{dT_{Ga}}{dt} = \frac{1}{m_{Ga} \cdot C_{p,Ga}} \cdot [Q_{cond,\mathrm{Ga}} - Q_{cond,\mathrm{Ga,}B} - Q_{cond,\mathrm{Ga,CF}} - Q_{cond,Sup}]$$

$$\frac{dT_{Ga}}{dt} = \frac{1}{m_{Ga} C_{p,Ga}} \cdot [\frac{\lambda_{Ga}}{L_{Ga}} \cdot S_{Ga} \cdot (T_{SS} - T_{Ga}) - \frac{\lambda_B}{L_B} \cdot S_{Ga} \cdot (T_{Ga} - T_B) - \frac{\lambda_{CF}}{L_{CF}} \cdot S_{Ga} \cdot (T_{Ga} - T_{CF}) - \frac{\lambda_{Sup}}{L_{Sup}} \cdot S_{Ga} \cdot (T_{Ga} - T_{Sup})]$$

where

- $Q_{cond,\mathrm{Ga,B}}$: Flow by conduction to Bakelite. It is a function Bakelite temperatures, the seal–Bakelite contact surface, the thickness of the rings, and the thermal conductivity of the Bakelite, defined as:

$$Q_{cond,Ga,B} = \frac{\lambda_B}{L_B} \cdot S_{Ga} \cdot (T_{Ga} - T_B)$$

- $Q_{cond,Ga,\mathrm{CF}}$: Flux by conduction to the ceramic fiber. It is a function of the temperatures, the joint-fiber contact surface, the thickness of the disk, and the thermal conductivity of the fiber. It is given by:

$$Q_{cond,Ga,\mathrm{CF}} = \frac{\lambda_{CF}}{L_{CF}} \cdot S_{Ga} \cdot (T_{Ga} - T_{CF})$$

- $Q_{cond,Ga,\mathrm{Sup}}$: In the absence of a specific insulating material between the joint and the substrate, the heat is transferred directly to the metal substrate. This flux is a function of the temperatures, the contact surface of the thickness of the support, and the thermal conductivity of the support:

$$Q_{cond,Ga,\mathrm{Sup}} = \frac{\lambda_{Sup}}{L_{Sup}} \cdot S_{Ga} \cdot (T_{Ga} - T_{Sup})$$

- Bakelite Insulating Rings: Bakelite Insulating Rings provide a lateral and peripheral thermal barrier between the stainless steel plate, the silicone gasket, and the bottom metal backing. Strategically placed around the cooking zone, they receive heat by conduction from the stainless steel plate and silicone seal, then transmit it to the lower support.

These rings do not participate in convective or radiative exchanges, as they are integrated into the internal structure of the device. Their main role is to limit lateral heat loss and protect the metal support from excessive overheating. The energy balance is based on the principle of energy conservation: the variation in the internal energy of the Bakelite is equal to the sum of the incoming flows (from the stainless steel and the gasket) minus the outgoing flow (to the support). It is given by:

$$\frac{dT_B}{dt} = \frac{1}{m_B \cdot C_{p,B}} \cdot [Q_{cond,\mathrm{SS,B}} + Q_{cond,Ga,\mathrm{B}} - Q_{cond,\mathrm{B},Ga}]$$

$$\frac{dT_B}{dt} = \frac{1}{m_B C_{p,B}} \cdot [\frac{\lambda_B}{L_B} \cdot S_{SS,B} \cdot (T_{BB} - T_B) + \frac{\lambda_B}{L_B} \cdot S_{Ga} . (T_{Ga} - T_B) - \frac{\lambda_{Ga}}{L_{Ga}} \cdot S_B \cdot (T_B - T_{Ga})]$$

where

- $Q_{cond,\mathrm{B},Ga}$: Heat flow exiting by thermal conduction to the steel support located under the rings. It is a function of the temperatures, the Bakelite–support contact surface, the thickness of the support, and the thermal conductivity of the steel support. It is given by:

$$Q_{cond,\mathrm{B},Ga} = \frac{\lambda_{Ga}}{L_{Ga}} \cdot S_B \cdot (T_B - T_{Ga})$$

- Insulating wool: Glass wool is the main insulation at the bottom of the cooker. It receives the heat by conduction from the heating element or ceramic fiber, and then transmits it to the lower support iron plate. The heat exchange model of the temperature of the glass wool is written as a function of the temperatures of the adjacent components (resistor, ceramic fiber, support, and iron plate), the heat fluxes received by conduction from the resistor and/or the fiber, and the heat flux transferred by conduction to the lower iron plate, by the expression:

$$\frac{dT_{GW}}{dt} = \frac{1}{m_{GW} C_{p,GW}} \cdot [Q_{cond,\mathrm{R,GW}} + Q_{cond,\mathrm{CF,GW}} - Q_{cond,\mathrm{GW,Ga}} - Q_{cond,\mathrm{GW,Fe}}]$$

$$\frac{dT_{GW}}{dt} = \frac{1}{m_{GW} C_{p,GW}} \quad [\frac{\lambda_{GW}}{L_{GW}} \cdot S_r \cdot (T_r - T_{GW}) + \frac{\lambda_{GW}}{L_{GW}} \cdot S_{CF,GW} \cdot (T_{CF} - T_{GW}) - \frac{\lambda_{Ga}}{L_{Ga}} . S_{GW,sup} . (T_{GW} - T_{Ga}) - \frac{\lambda_{Fe}}{L_{Fe}} . S_{Fe} . (T_{GW} - T_{Fe})]$$

where

- $Q_{cond,\mathrm{CF},GW}$: Conductive heat transfer where the wool receives heat by conduction from the fiber disk placed above it. It is a function of the temperatures, the

fiber–wool contact surface, the wool thickness, and the thermal conductivity. It follows the relation:

$$Q_{cond,CF,\mathrm{GW}} = \frac{\lambda_{GW}}{L_{GW}} \cdot S_{CF,GW} \cdot (T_{CF} - T_{GW})$$

- $Q_{cond,GW,Sup}$: Heat flow lost by thermal conduction from the wool to the metal support (steel sheet) located laterally. This flow represents a lateral heat loss. It is a function of the temperatures, the wool–support contact surface, the thickness of the support, and the thermal conductivity of the steel support:

$$Q_{cond,GW,\mathrm{Sup}} = \frac{\lambda_{Sup}}{L_{Sup}} . S_{GW,Sup} . (T_{GW} - T_{Sup})$$

- $Q_{cond,\mathrm{GW,Fe}}$: Heat flow exiting by thermal conduction to the iron plate constituting the bottom of the cooker. This flux represents the final heat losses to the outside of the system. It is a function of the temperatures, the wool–iron contact surface, the thickness of the iron plate, and the thermal conductivity of the iron. It is expressed as:

$$Q_{cond,\mathrm{GW,Fe}} = \frac{\lambda_{Fr}}{L_{Fr}} . S_{Fr} . (T_{GW} - T_{Fr})$$

- Ceramic fiber: Ceramic fiber is a high-temperature insulation layer located between the resistor, the stainless steel plate, the gasket, and the glass wool. It receives heat by conduction from these three components and then transmits it to the bottom support and the insulating wool.

Thanks to its very low thermal conductivity and resistance to more than 1200 °C, it plays a key role in reducing heat loss while withstanding high temperatures close to the resistance. The heat exchange model of the temperature of the ceramic fiber is written as a function of the temperatures of the adjacent components (resistor, stainless steel plate, silicone gasket, metal support, and glass wool), the heat fluxes received by conduction from the resistor, the stainless steel plate, and the gasket, and the heat flows transferred by conduction to the support and the wool, by the expression $(T_{CF} T_r T_{SS} T_{Ga} T_{Sup} T_{GW})$:

$$\frac{dT_{CF}}{dt} = \frac{1}{m_{CF} C_{p,CF}} \cdot [Q_{cond,CF} + Q_{cond,SS,CF} + Q_{cond,Ga,CF} - Q_{cond,CF,\mathrm{Ga}} - Q_{cond,CF,GW}]$$

$$\begin{aligned} \frac{dT_{CF}}{dt} = \frac{1}{m_{CF} C_{p,CF}} \quad & [\tfrac{\lambda_{CF}}{L_{CF}} \cdot S_r \cdot (T_r - T_{CF}) + \tfrac{\lambda_{CF}}{L_{CF}} \cdot S_{SS,CF} \cdot (T_{SS} - T_{CF}) + \tfrac{\lambda_{CF}}{L_{CF}} \cdot S_{Ga} \cdot (T_{Ga} - T_{CF}) \\ & - \tfrac{\lambda_{Sup}}{L_{Ga}} . S_{CF,Sup} . (T_{CF} - T_{Sup}) - \tfrac{\lambda_{GW}}{L_{GW}} . S_{CF,GW} . (T_{CF} - T_{GW})] \end{aligned}$$

where

- $Q_{cond,\mathrm{CF,Sup}}$: Heat flow lost by thermal conduction from the fiber to the steel support located laterally or peripherally. This flow represents a lateral heat loss to the metal structure of the cooker. It is a function of the temperatures, the fiber–support contact surface, the thickness of the support, and the thermal conductivity of the support:

$$Q_{cond,\mathrm{CF,Sup}} = \frac{\lambda_{Sup}}{L_{Sup}} . S_{CF,Sup} . (T_{CF} - T_{Sup})$$

- $Q_{cond,\mathrm{CF,GW}}$: Heat flow lost by thermal conduction from the fiber to the glass wool layer underneath. This flow represents the main vertical heat loss to the bottom of the cooker. It is a function of the temperatures, the fiber–wool contact surface, the thickness of the wool, and the thermal conductivity of the wool:

$$Q_{cond,\mathrm{CF,GW}} = \frac{\lambda_{GW}}{L_{GW}}.S_{CF,GW}.(T_{CF} - T_{GW})$$

- Iron Bottom Plate: The iron bottom plate is the lower outer shell of the cooker. It receives heat by conduction from the glass wool, and represents the last link in the heat loss of the system. Its temperature remains low, but it contributes to the residual heat dissipation. The heat exchange model of the temperature of the iron plate is written as a function of the temperature of the glass wool located above, the reference temperature for radiation, the heat flux received by conduction from the wool, and the heat fluxes lost by natural convection and thermal radiation to the external environment by the expression:

$$\frac{dT_{Fe}}{dt} = \frac{1}{m_{Fe}C_{p,Fe}}\cdot[Q_{cond,SS,Fe} - Q_{conv,Fe,A} - Q_{rad,Fe,A}]$$

$$\frac{dT_{Fe}}{dt} = \frac{1}{m_{Fe}C_{p,Fe}} \quad [\frac{\lambda_{Fe}}{L_{Fe}}.S_{Fe}.(T_{SS} - T_{Fe}) - h_{cv}.S_{Fe}.(T_{Fe} - T_{amb}) - \sigma.\mathcal{E}_{Fe}.S_{Fe}.[(T_{Fe} + 273)^4 - (T_c + 273)^4]]$$

where

- $Q_{conv,\mathrm{Fe},A}$: Heat losses by natural convection between the lower surface of the iron plate and the ambient air. They are calculated according to the temperatures, the exposed surface, and the natural convection coefficient for a hot surface facing downwards ($T_{Fe} - T_{amb}$), S_{Fe}, h_{cv_b}):

$$Q_{conv,Fe,A} = h_{cv\_b}.S_{Fe}.(T_{Fe} - T_{amb})$$

- $Q_{rad,Fe,A}$: Thermal losses by infrared radiation between the surface of the iron plate and the environment according to the Stefan–Boltzmann law. They are calculated as a function of the absolute temperatures, the surface area, the emissivity of the iron, and the Stefan–Boltzmann constant [28]:

$$Q_{rad,Fe,A} = \sigma.\mathcal{E}_{Fe}.S_{Fe}.\left[(T_{Fe} + 273)^4 - (T_c + 273)^4\right]$$

- Bracket: The steel bottom bracket is the main mechanical structure of the photovoltaic solar cooker. It receives heat by conduction from the joint, Bakelite, glass wool, and ceramic fiber. It transmits this heat to the outside by natural convection to the ambient air and by thermal radiation to the environment.

It represents the final exit point for residual heat losses. Its temperature remains moderate, but it plays a key role in the overall dissipation. The energy balance is based on the principle of energy conservation: the variation in the internal energy of the medium is equal to the sum of the incoming flows minus the outgoing flows. follows the relation:

$$\frac{dT_{Sup}}{dt} = \frac{1}{m_{Sup}C_{p,Sup}}\cdot[Q_{cond,Ga,Sup} + Q_{cond,SS,Sup} + Q_{cond,CF,Sup} + Q_{cond,B,Sup} - Q_{cond,Sup,\mathrm{A}} - Q_{rad,Sup,\mathrm{A}}]$$

$$\frac{dT_{Sup}}{dt} = \frac{1}{m_{Sup}C_{p,Sup}} \quad [\frac{\lambda_{Sup}}{L_{Sup}}\cdot S_{Ga}\cdot(T_{Ga} - T_{Sup}) + \frac{\lambda_{Sup}}{L_{Sup}}\cdot S_{SS,Sup}\cdot\left(T_{SS} - T_{Sup}\right) + \frac{\lambda_{Sup}}{L_{Sup}}\cdot S_{CF,Sup}\cdot(T_{CF} - T_{Sup}) + \frac{\lambda_{Sup}}{L_{Sup}}\cdot S_B\cdot(T_B - T_{Sup}) - h_{cv}\cdot S_{Sup\ total}\cdot(T_{Sup} - T_{amb}) - \sigma\cdot\mathcal{E}_{Sup}\cdot S_{Sup\ total}\cdot\left[(T_{Sup} + 273)^4 - (T_c + 273)^4\right]]$$

where

- $Q_{cond,Sup,A}$: heat flux lost by natural convection between the substrate and the ambient air (W)

$$Q_{cond,Sup,A} = h_{cv} \cdot S_{Sup\ total} \cdot (T_{Sup} - T_{amb})$$

- $Q_{rad,Sup,A}$: The substrate emits infrared thermal radiation from its exposed surfaces according to the Stefan–Boltzmann law:

$$Q_{rad,Sup,A} = \sigma \cdot \varepsilon_{Sup} \cdot S_{Sup\ total} \cdot \left[(T_{Sup} + 273)^4 - (T_c + 273)^4 \right]$$

- Glass teapot: The borosilicate glass teapot is placed directly on the stainless steel plate. Its glass bottom is the heat transfer interface between the cooking surface and the water contained, it receives heat by conduction from the stainless steel plate, then transmits it to the water by natural convection at the glass-water interface. The energy balance is based on the principle of energy conservation: the variation in the internal energy of the glass bottom is equal to the incoming flow (from the stainless steel) minus the outgoing flow (to the water). can be formulated as:

$$\frac{dT_G}{dt} = \frac{1}{m_G C_{p,G}} \cdot [Q_{cond,SS,G} - Q_{conv,G,Water} - Q_{cond,G,A} - Q_{rad,G,A}]$$

$$\frac{dT_G}{dt} = \frac{1}{m_G C_{p,G}} \cdot \left[\frac{\lambda_G}{L_G} \cdot S_G \cdot (T_{SS} - T_G) - h_{cv} \cdot S_G \cdot (T_G - T_{Water}) - h_{cv} \cdot S_{G\ total} \cdot (T_G - T_{amb}) - \sigma \cdot \varepsilon_G \cdot S_{G\ total} \cdot [(T_G + 273)^4 - (T_c + 273)^4] \right]$$

where

- $Q_{conv,G,Water}$: This heat flux represents the useful energy transmitted to the fluid to be heated and is expressed by the following relationship:

$$Q_{conv,G,Water} = h_{cv} . S_G . (T_G - T_{Water})$$

- Water is the target fluid of the photovoltaic solar cooker. It receives heat by convection from the glass bottom of the teapot, then dissipates it to the environment by natural convection, evaporation, and thermal radiation. The thermal behavior of water is closely dependent on the temperature of the glass bottom, the ambient conditions and the lid. Its development is described on the basis of an energy balance based on the principle of energy conservation.

$$\frac{dT_{Water}}{dt} = \frac{1}{m_{Water} C_{p,Water}} \cdot [Q_{conv,G,Water} - Q_{conv,Water,A} - Q_{evap,Water,A} - Q_{rad,Water,A}]$$

$$\frac{dT_{Water}}{dt} = \frac{1}{m_{Water} C_{p,Water}} \cdot [h_{cv} \cdot S_G \cdot (T_F - T_{Water}) - h_{cv} \cdot S_G \cdot (T_{Water} - T_{cond}) - h_{ev} \cdot S_G \cdot (T_{Water} - T_{cond}) - \sigma \cdot \varepsilon_{eff} \cdot S_G \cdot [(T_{Water} + 273)^4 - (T_{cond} + 273)^4]]$$

where

- $Q_{conv-eau\_air}$ This heat flux represents an energy loss due to convective exchanges between the free surface of the water and the ambient air or the lid. It is expressed by the following relation:

$$Q_{conv,Water,A} = h_{cv} \cdot S_G \cdot (T_{Water} - T_{cond})$$

Evaporation is a major mode of energy loss when the water temperature approaches 100 °C. It is modeled by a heat flux proportional to the temperature and vapor pressure gradient [28]:

$$Q_{evap,Water,A} = h_{ev} \cdot S_G \cdot (T_{Water} - T_{cond})$$

where

- ✓ h_{ev}: Evaporative heat transfer coefficient ($W/m^2 \cdot K$). It is calculated by the relationship [26,29]:

$$h_{ev} = 16.273 \times 10^{-3} \cdot h_{cv} \cdot \left[\frac{P_{Water} - P_{cond}}{T_{Water} - T_{cond}}\right]$$

- $Q_{rad,Water,A}$: Heat flux lost by radiation between the water surface and the air/cover (W). It is defined as:

$$Q_{rad,Water,air} = \sigma \cdot \varepsilon_{eff} \cdot S_G \cdot [(T_{Water} + 273)^4 - (T_{cond} + 273)^4]$$

3.3. Resolution Methodology and Simulation Environment

In our simulation, the Runge–Kutta method of order 4 (RK4) was used, being one of the most widespread numerical techniques for solving ordinary differential equations (ODEs). This approach is particularly suitable for the analysis of thermal dynamical systems, offering an efficient trade-off between numerical accuracy and stability. It is therefore an excellent compromise between simplicity of implementation, numerical stability and precision [30]. Its principle is based on the approximation of the solution of an EDO using a weighted combination of several evaluations of the derived function (or slope) at different points in the time interval. In contrast to the explicit Euler method, which performs only one evaluation per step, the RK4 method performs four intermediate evaluations. This makes it possible to achieve significantly higher accuracy, even with relatively wide time steps. The classical formulation (1) of the Runge–Kutta method of order 4 is written [30]:

$$\begin{cases} K^{(1)} = F(y^n, t^n) \\ K^{(2)} = F(y^n + \frac{\Delta t}{2} K^{(1)}, t^n + \frac{\Delta t}{2}) \\ K^{(3)} = F(y^n + \frac{\Delta t}{2} K^{(2)}, t^n + \frac{\Delta t}{2}) \\ K^{(4)} = F\left(y^n + \Delta t \cdot K^{(3)}, t^n + \Delta t\right) \\ y^{n+1} = y^n + \frac{\Delta t}{6}[K^{(1)} + 2K^{(2)} + 2K^{(3)} + K^{(4)}] \end{cases}$$

This formulation is based on four successive estimates of the slope, denoted $K^{(1)}$, $K^{(2)}$, $K^{(3)}$, and $K^{(4)}$. These are obtained by evaluating the function at different intermediate instants within the time step Δt. The weighted combination of these estimates provides an accurate and stable approximation of the solution. $K^{(1)}K^{(2)}K^{(3)}K^{(4)}F(y^n, t^n)y^{n+1}$.

Thus, the RK4 method stands out for its efficiency and robustness, which explains its widespread use in the numerical modeling of dynamical systems. To implement this model and solve ordinary differential equations (ODEs) using the 4th order Runge–Kutta numerical method (RK4), we used the Python language. This choice is justified by the flexibility of the language, the simplicity of its syntax, as well as the availability of high-performance scientific libraries such as NumPy, SciPy, Matplotlib (version 3.10) or SymPy. These tools offer the ability to model the physical equations of the system, solve them numerically, and visualize the results efficiently. To numerically solve the model of the photovoltaic solar cooker, a simulation code was developed in Python (Figure 5). This code adopts a modular and hierarchical structure, facilitating the modeling of the thermal evolution of the different components of the system, including:

- The heating element
- The heating plate (metal support)
- The water in a teapot

The program developed makes it possible to simulate the temperature rise in each component of the system as a function of time, taking into account different thermal insulation configurations. It is based on the numerical solution of heat transfer equations by conduction, convection and radiation. As shown in Figure 6, the implemented algorithm performs the following steps:

- Reading of input data and initial conditions: available thermal power, ambient temperature, as well as the thermo-physical and geometric properties of the materials making up the system (stainless steel, insulation, etc.).
- Calculation of the time step to make the time simulation evolve.
- Evaluation of convection heat transfer coefficients at each iteration, as a function of surface and temperature conditions. Thermal properties, such as specific heats and conductivities, are then updated to reflect their possible variations with temperature.
- Calculation of the temperatures of each element of the system from the energy equilibrium equations. This process repeats until the maximum time set by the user is reached.
- Analysis of the results: the evolution of the temperatures in the different zones of the device is studied, the thermal losses according to the three modes of transfer are evaluated, and the thermal performance of the different insulation configurations is compared.

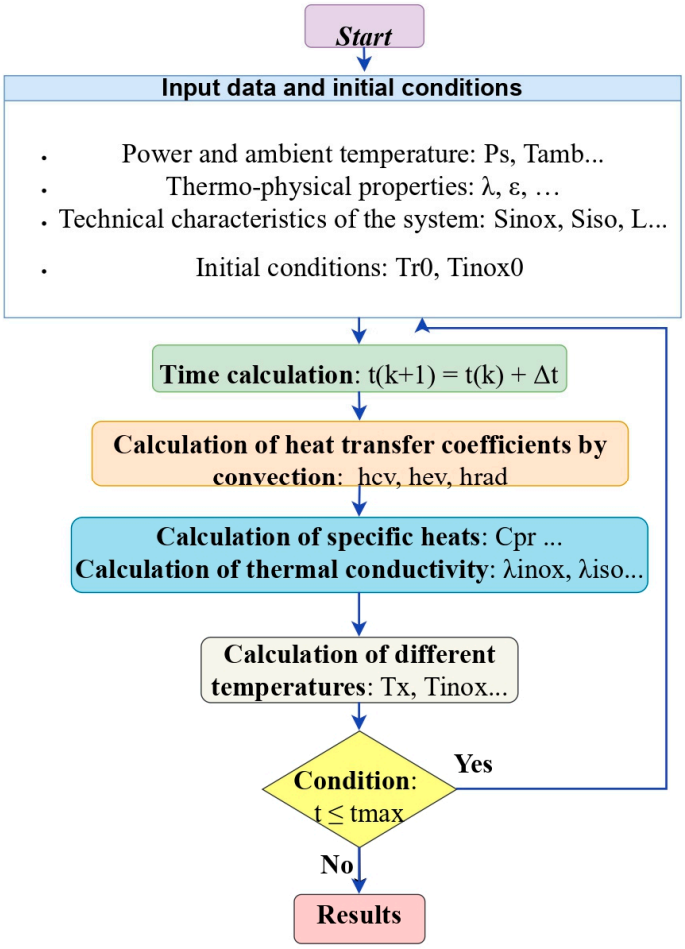

Figure 6. Diagram of the algorithm for simulating the temperatures of the heating plate and the water to be heated.

4. Setup and Methodology of the Solar Cooker

The practical tests were carefully selected to reflect the real-world operating conditions of the solar cooker, taking into account typical household usage in sunny regions such as Africa. Representative scenarios, including water heating (boiling) and the preparation of common dishes, were therefore integrated to ensure that the results are relevant and consistent with domestic practices. In particular, the water boiling test was chosen as a reference experiment, as it is widely used in the literature and enables direct and standardized comparison with other solar and conventional cookers. This approach guarantees that the experimental results accurately reflect daily usage conditions while also facilitating meaningful performance benchmarking.

4.1. Measuring Bench

Figure 7 illustrates all the equipment of the prototype solar cooker, installed at the LETSER laboratory of Mohammed Premier University in Oujda (Morocco). The proposed cooker is designed to produce a total energy of between 2 and 4.5 kWh per day. The main components of the system and the devices required for its operation and testing are described below:

- Photovoltaic (PV) panels—1200 Wp: Two PV panels (1) connected in series, with a total output of 600 Wp, are connected directly to the control box (10). They produce a useful cooking energy of between 1 and 2.5 kWh/day. Two further PV panels (2) mounted in series (600 Wp) are connected to the solar batteries (5) via the charge/discharge controller (4), ensuring battery charging and a cooking energy of 1 to 2 kWh/day.
- Solar Batteries (5): The system consists of four 12 V/250 Ah batteries mounted in series, forming a 48 V/250 Ah assembly. They are charged by the PV panels (2) via the controller (4) and can store up to 12 kWh of energy. Depending on the cooking needs, they can provide 1 to 1.2 kWh/day of useful energy.
- Energy Control and Management Box (10): This box receives energy from the PV panels (1) and batteries (5). It regulates and distributes power to the heating plate (11) using two DC/DC converters, controlled by an electronic control board. This board, based on a Raspberry Pi PICO microcontroller, provides complete cooker supervision, automatic switching of power sources (PV/battery), and overall operation safety.
- Heating plate (11) consists of two resistors (left and right), each of which can reach a maximum power of 2 kW and an operating temperature of up to 1000 °C. It is the main cooking element of the solar cooker.
- Meteorological station (8) comprises a pyranometer (3) and a thermal sensor, for measuring solar irradiance and ambient temperature. These measurements are essential to correlate the sunlight conditions with the thermal performance of the cooker.
- A computer, combined with two display screens, allows the control board to be programmed, the operating parameters to be adjusted, and the performance of the cooker to be monitored in real time via the application developed for this work, both locally and remotely via the Internet. The application continuously monitors the electrical quantities (voltages, currents, and powers of each converter) as well as the temperatures of the sheet metal, the heating elements, and the cooking zone. The data is transmitted via the MQTT HiveMQ broker, guaranteeing real-time monitoring of thermal and electrical evolution and contributing to the optimization of the system's energy efficiency.

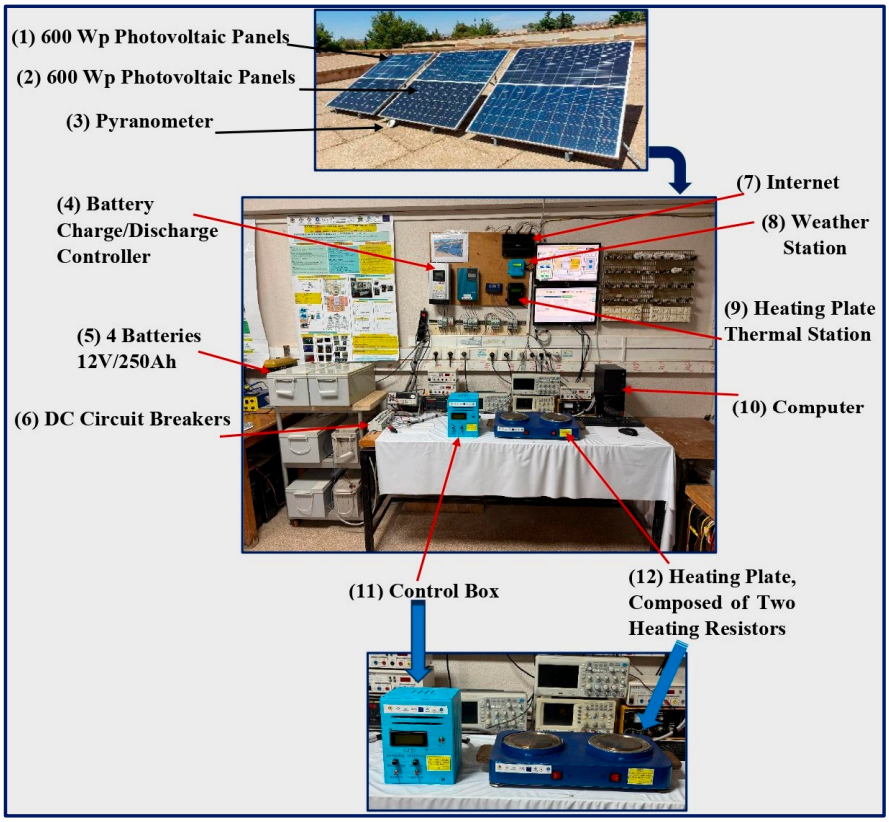

Figure 7. Measuring bench for the test of the solar cooker developed as part of this work.

4.2. Stage of Realization of the Control Box

The realization of the control box followed several methodical steps, from mechanical design to full electronic integration, as illustrated in Figure 8:

- Mechanical design: 3D modeling of the box and its internal support using Tinkercad software (latest version at the time of the study, available at https://www.tinkercad.com/, accessed on 2 September 2025). This phase made it possible to define the precise location of each electronic component and to ensure an optimal layout for wiring, ventilation, and maintenance. Once the design was validated, the physical manufacturing was carried out using Creality Ender S1 3D printer (manufacturer: Creality, purchased from a supplier in Temara, Morocco) with a PLA filament, offering good mechanical and thermal resistance. The result is a rigid, compact structure that is perfectly suited to the experimental conditions of the laboratory.
- Mounting and wiring the electronic boards: After printing, we mounted and wired the electronic boards to the printed media. It hosts four main maps, each serving a specific function:
  - Two boost-type DC/DC converters: one dedicated to the power supply from photovoltaic (PV) panels and the other to that of batteries;
  - A control board, controlled by the Raspberry Pi, ensuring the regulation of the system and the transmission of data;
  - A switch card to select the power source used: PV, battery, or both simultaneously.
- Integration of the control and display elements: Once the boards were fixed and interconnected, we integrated the control and display elements into the box: PV and PROOF switches, control knobs, a LCD 2004 screen, and a buzzer for audible alerts. The internal wiring has been carefully designed to ensure the electrical reliability, safety, and ease of maintenance of the device.

- Final assembly: Finally, the electronic support was integrated into the printed box, constituting a complete, functional, and esthetically accomplished system. This control box represents the heart of the solar cooker's energy management system, ensuring the regulation, real-time monitoring, and protection of the entire device.

4.3. Stage of Making the Heating Plate

As shown in Figure 9, the production and wiring of the heating plate follows several successive steps:

- Development of the heating plate: The plate is made from a metal sheet, laser-drilled to accommodate the resistors, contact sockets, switches and LEDs.
- Installation of heating elements: Two 18 Ω resistors are attached to the metal sheet, which serves as both a mechanical support and a thermal diffusion surface. To ensure optimal insulation and prevent heat dissipation by conduction, Bakelite rings (front side) and ceramic fiber disks (back side) were used. These materials, known for their stability at high temperatures (up to 1200 °C), provide effective protection between the resistors and the sheet. Two ceramic fiber disks are thus interposed to eliminate direct contact and enhance the thermal performance of the device.
- Additional insulation: The whole plate is covered with a layer of glass wool, acting as additional insulation to limit heat loss to the lower part of the system. This arrangement helps to concentrate the heat flow to the useful cooking surface, improving the overall energy efficiency of the cooker.
- Protective cover: A metal cover closes the plate from below, ensuring mechanical safety, protection of internal components, and structural stability of the whole plate.

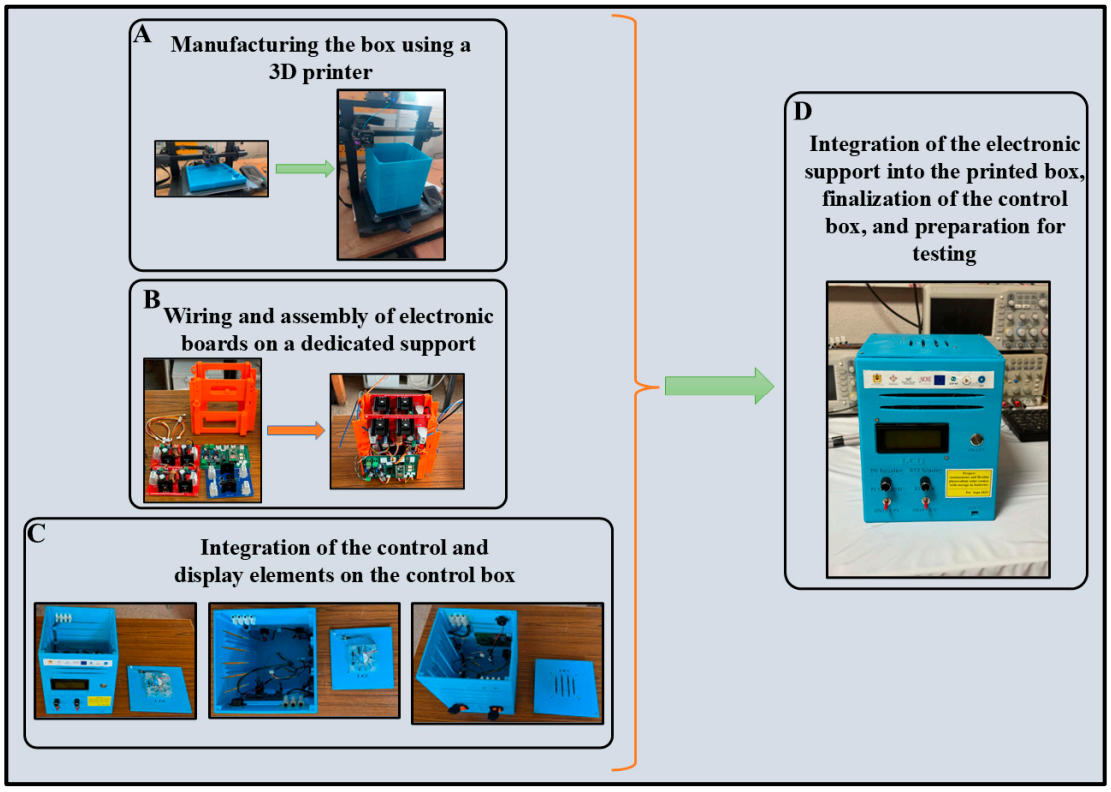

Figure 8. Steps for making the control box. (**A**): Manufacturing the box using a 3D printer. (**B**): Wiring and assembly of electronic boards on a dedicated support. (**C**): Integration of the control and display elements on the control box. (**D**): Integration of the electronic support into the printed box, finalization of the control box, and preparation for testing.

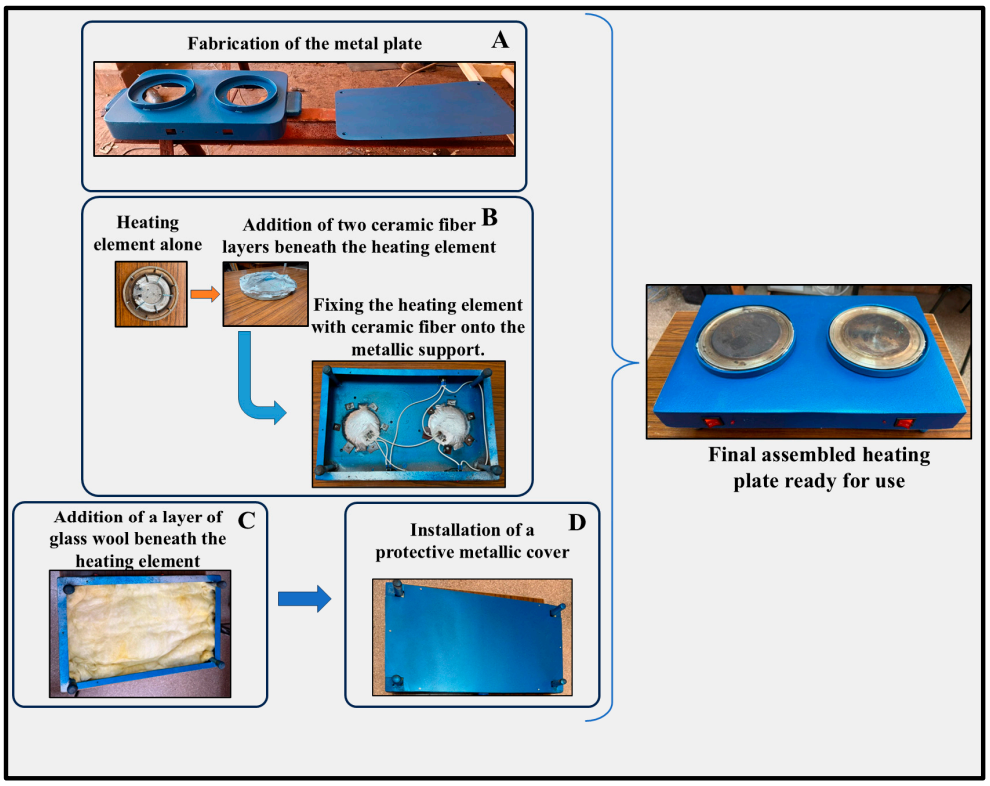

Figure 9. Steps to make the heating plate. (**A**): Fabrication of the metal plate. (**B**): Fixing the heating element with ceramic fiber onto the metallic support. (**C**): Addition of a layer of glass wool beneath the heating element. (**D**): Installation of a protective metallic cover.

5. Experimental Results

5.1. Thermal Model Validation

In this section, we proceed to the experimental validation of the theoretical and thermal models of the photovoltaic solar cooker developed during this work (Figure 7). This validation focuses more particularly on the evolution of the characteristic temperatures of the system, namely the temperature of the heating resistor, the temperature of the sheet of the heating plate, and the temperature corresponding to the boiling of the water. The experimental tests were carried out when the cooker is powered either directly by the photovoltaic panels or by the storage batteries, in order to evaluate the thermal behavior in both operating modes.

As specified in the section on theoretical modeling, the parameters and constants used in the simulations were determined from the data in the literature [31] and adjusted according to the actual characteristics of the cooker. These parameters include the ambient temperature Tamb, the nominal electrical power Ps, the gravitational constant g, the Stefan–Boltzmann constant σ, and the geometric and thermophysical properties of the individual components: surfaces, thicknesses, masses, thermal conductivity, heat capacity, and emissivity. These values, grouped in Table 1, make it possible to faithfully reproduce the experimental conditions and to characterize the heat transfers by conduction, convection, and radiation within the system.

Table 1. Input data and physical parameters used for the thermal modeling of the photovoltaic solar cooker.

Parameter	Symbol	Value	Unit
Coefficient C	C	0.15	–
Specific heat capacity of glass	$C_{p,G}$	900	J/kg · K
Specific heat capacity of the resistor	$C_{p,r}$	445	J/kg · K
Specific heat capacity of water	$C_{p,Water}$	4186	J/kg · K
Effective emissivity for resistor	$\varepsilon_{eff,r}$	0.8	–
Painted iron emissivity	ε_{Fe}	0.7	–
Glass emissivity	ε_{G}	0.9	–
Polished stainless steel emissivity	ε_{SS}	0.25	–
Painted steel emissivity	ε_{Sup}	0.7	–
Water emissivity	ε_{Water}	0.95	–
Thick Bakelite rings	L_B	10×10^{-3}	m
Ceramic fiber thickness	L_{CF}	10×10^{-3}	m
Thickness iron plate	L_{Fe}	2×10^{-3}	m
Thickness teapot bottom	L_G	3×10^{-3}	m
Thickness silicone seal	L_{Ga}	65×10^{-3}	m
Glass wool thickness	L_{GW}	35×10^{-3}	m
Thickness of stainless steel plate	L_{SS}	2×10^{-3}	m
Steel support thickness	L_{Sup}	3×10^{-3}	m
Thermal conductivity of glass	λ_G	1.2	W/m · K
Bakelite mass	m_B	0.15	Kg
Ceramic fiber mass	m_{CF}	0.02	Kg
Iron plate mass	m_{Fe}	0.25	Kg
Teapot mass	m_G	0.250	Kg
Silicone gasket mass	m_{Ga}	0.02	Kg
Glass wool mass	m_{GW}	0.01	Kg
Resistance mass	m_r	0.09	Kg
Stainless steel plate mass	m_{SS}	0.1	Kg
Steel support mass	m_{Sup}	5	Kg
Water mass	m_{Water}	1	Kg
Coefficient n	n	1/3	–
Gravity	g	9.81	m/s^2
Rated electrical power	P_s	350	W
Bakelite surface	S_B	0.016	m^2
Ceramic fiber surface	S_{CF}	0.022	m^2
Fiber–support contact surface	$S_{CF,Sup}$	0.012	m^2

Table 1. *Cont.*

Parameter	Symbol	Value	Unit
Iron contact surface	S_{Fe}	0.035	m^2
Glass contact surface	S_G	0.015	m^2
Ring surface silicone gasket	S_{Ga}	0.012	m^2
Glass wool–support contact surface	$S_{GW,Sup}$	0.025	m^2
Resistor exchange surface	S_r	0.004	m^2
Surface of the stainless steel plate	S_{SS}	0.025	m^2
Stefan–Boltzmann constant	σ	5.67×10^{-8}	$W/m^2 \cdot K^4$
Ambient temperature	T_{amb}	27	°C

5.2. Empty Experimentation

In this case, we carried out the thermal experimentation and simulation of the vacuum cooker, i.e., without load applied to the heating element, in order to analyze its thermal behavior in two configurations, without insulation and with insulation.

- Without insulation: Figure 9 shows the temporal evolution of the temperatures from numerical simulation and experimental measurements in the case of no-load operation. To avoid any confusion, the stainless steel plate is referred to as a coil, since it is directly attached to the heating element. The results show that the temperature of the resistor tends towards a stabilization value of about 318 °C, while the plate (sheet in direct contact with the resistor) reaches about 60 °C, both experimentally and numerically. This concordance between simulation and experimentation confirms the validity of the numerical model. The simulation also provides a better understanding of the internal thermal behavior of the system, clearly distinguishing between heat generation at the resistance level and its gradual diffusion to the hob. It should be noted that, in this initial configuration, the system is completely open from the bottom, thus leading to a significant dissipation of energy to the environment. In addition, the direct contact between the resistor and the sheet causes heat transfer without an insulating barrier, accentuating heat losses. This reference situation highlights the need to integrate an insulation material to improve the energy efficiency of the device.
- With insulation:
  The study of the different thermal insulation configurations of the heating plate made it possible to evaluate the influence of insulating materials on heat distribution and containment. Vacuum tests were carried out in order to simulate and experiment with the temperature distribution at critical points in the system, particularly at the level of strength and metal sheet.
  - ✓ First configuration: Bakelite alone. A Bakelite disk was inserted between the resistor and the sheet, without the addition of glass wool, in order to evaluate the insulating capacity of the Bakelite and eliminate direct contact between the two elements. As shown in Figure 10, the measurements indicate a slight improvement in thermal confinement, with a temperature of the resistance reaching about 355 °C, a notable increase compared to the case without insulation. However, due to its relatively high thermal conductivity and low heat resistance (≈200–250 °C), Bakelite quickly showed signs of degradation (browning and loss of stiffness). This configuration therefore proved insufficient for prolonged operation.

- ✓ Second configuration: Bakelite + glass wool. In this configuration, a Bakelite disk was placed between the resistor and the sheet metal, while a layer of glass wool was added in the lower part to reduce downward heat losses. The experimental results (Figure 10) show a significant increase in the temperature of the resistor, reaching about 500 °C, an increase of nearly 156% compared to the reference case. This improvement reflects a significant reduction in heat losses and improved energy efficiency of the system. However, the temperature obtained greatly exceeds the thermal limit of Bakelite, causing it to degrade and burn. This underscores the need for an insulating material that can withstand higher temperatures.
- ✓ Third configuration: ceramic fiber + glass wool. In order to overcome the limitations of Bakelite, it has been replaced by ceramic fiber, known for its high thermal resistance (up to 1200 °C). Two ceramic fiber disks were inserted to eliminate any direct contact between the strength and the sheet, and a layer of glass wool was added underneath to reinforce the overall insulation. The experimental results (Figure 10) show a resistance temperature of about 518 °C, while the sheet remains close to 58 °C, reflecting excellent thermal confinement. Numerical simulations confirm these observations. Unlike previous cases, no degradation or odor emission was observed, attesting to the reliability and durability of the material. This final configuration, combining ceramic fiber and glass wool, allows for an improvement of approximately 163% in the firing temperature compared to the case without insulation, thus demonstrating a significant gain in energy performance and thermal stability of the system.

All the results obtained show an excellent agreement between the theoretical models presented above and the experimental measurements, with deviations of less than 5% in all the cases studied. When empty, and independently of the experimental scenario (with or without insulation), the thermal behavior of the cooker is reproduced well by the simulation, confirming the validity of the model developed. The maximum temperature of the heating element of around 518 °C is reached with the combination of ceramic fiber and glass wool. This clear improvement is the result of the heat containment around the strength: ceramic fiber, characterized by very low thermal conductivity and excellent resistance to high temperatures (up to 1200 °C), effectively limits conduction losses, while glass wool reduces thermal leakage to the base. This allows the heat flow to be concentrated to the hob, increasing the energy efficiency of the system.

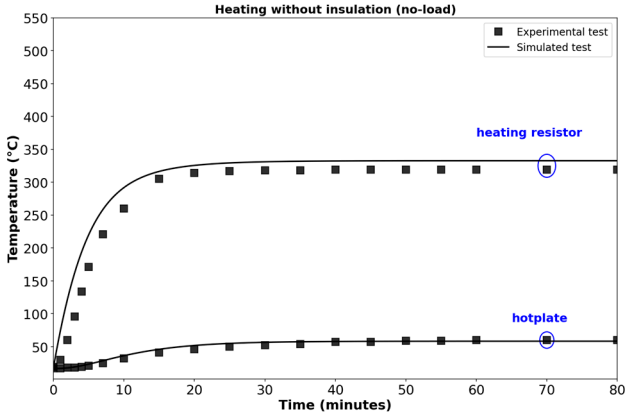

Figure 10. Temporal analysis without isolation: simulation and experimentation.

Compared to configurations using Bakelite alone or in combination with glass wool, the use of ceramic fiber allows for an increase of approximately 60 to 65% in the temperature of the resistor.

As a result, the photovoltaic solar cooker developed in this work has remarkable thermal performance when empty, making it particularly suitable for cooking applications requiring high temperatures.

In the following paragraph, we analyze the behavior of the cooker when heating a liter of water, in order to evaluate its performance in real cooking conditions.

5.3. Water Heating: Thermal Behavior of the Plate in Operation

In this part, we analyze the thermal behavior of the cooker when heating a liter of water, comparing the results obtained experimentally and numerically, with and without insulation. These tests aim to evaluate the influence of insulation on the temperature distribution and on the time required for water to boil, a parameter representative of the energy efficiency of the system:

- Without insulation: Figure 11 shows the temporal evolution of the temperatures from numerical simulation and experimental measurements when heating a liter of water without insulation. The temperature of the resistor stabilizes around 240 °C, while the metal sheet in direct contact reaches about 60 °C in both approaches. The water reaches its boiling point after about 48 min. The agreement between the simulated and measured results confirms the relevance of the numerical model and its ability to faithfully reproduce the thermal behavior of the cooker. However, the lack of insulation leads to significant heat losses to the environment, resulting in a relatively long boiling time.
- With insulation: In order to evaluate the impact of different insulating materials on thermal performance, several configurations were tested by measuring the temperature of the resistance and that of the sheet, as well as the boiling time of the water.
  - ✓ First configuration: Bakelite alone. A Bakelite disk was inserted between the resistor and the metal sheet, without the addition of glass wool. As shown in Figure 12, the temperature of the resistor stabilizes around 300 °C, while the sheet reaches about 50 °C in both approaches. The water reaches a boil after 38 min, reflecting a slight improvement in thermal efficiency compared to the case without insulation.
  - ✓ Second configuration: Bakelite + glass wool. The combination of Bakelite and glass wool aims to strengthen the confinement of heat. The experimental results (Figure 12) show a noticeable increase in the temperature of the resistor, reaching about 340 °C, while the sheet remains around 45 °C. The boiling time of the water is reduced to about 27 min, which indicates a significant improvement in the energy efficiency of the cooker.
  - ✓ Third configuration: ceramic fiber + glass wool. In this optimized configuration, the Bakelite is replaced by ceramic fiber, a highly heat-resistant material. As indicated by the experimental results (Figure 13), the temperature of the resistance reaches about 345 °C, while the sheet remains stable around 45 °C, confirming an excellent thermal confinement. The water then reaches its boiling point after just 23 min, a reduction of almost 52% in cooking time compared to the case without insulation. Numerical simulations faithfully reproduce these results, validating the thermal performance of the model and the superiority of this configuration.

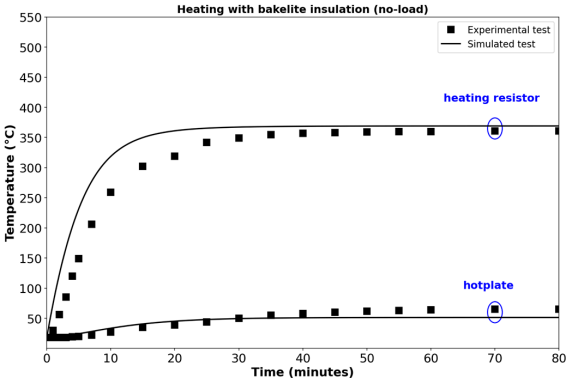

(**A**)

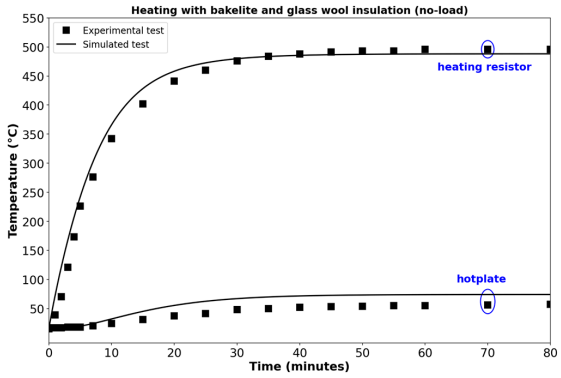

(**B**)

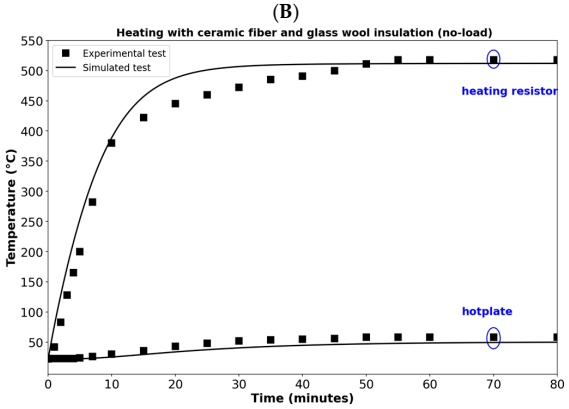

(**C**)

Figure 11. Temporal analysis of temperatures for different vacuum insulation configurations: simulation and experimentation. (**A**): Heating with Bakelite insulation (no-load). (**B**): Heating with Bakelite and glass wool insulation (no-load) (**C**): Heating with ceramic fiber and glass wool insulation (no-load).

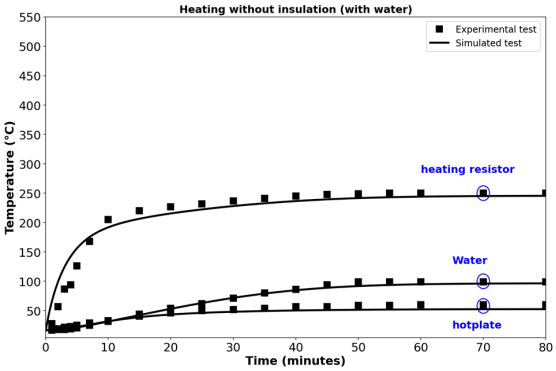

Figure 12. Temporal analysis of temperatures when heating a liter of water without insulation: simulation and experimentation.

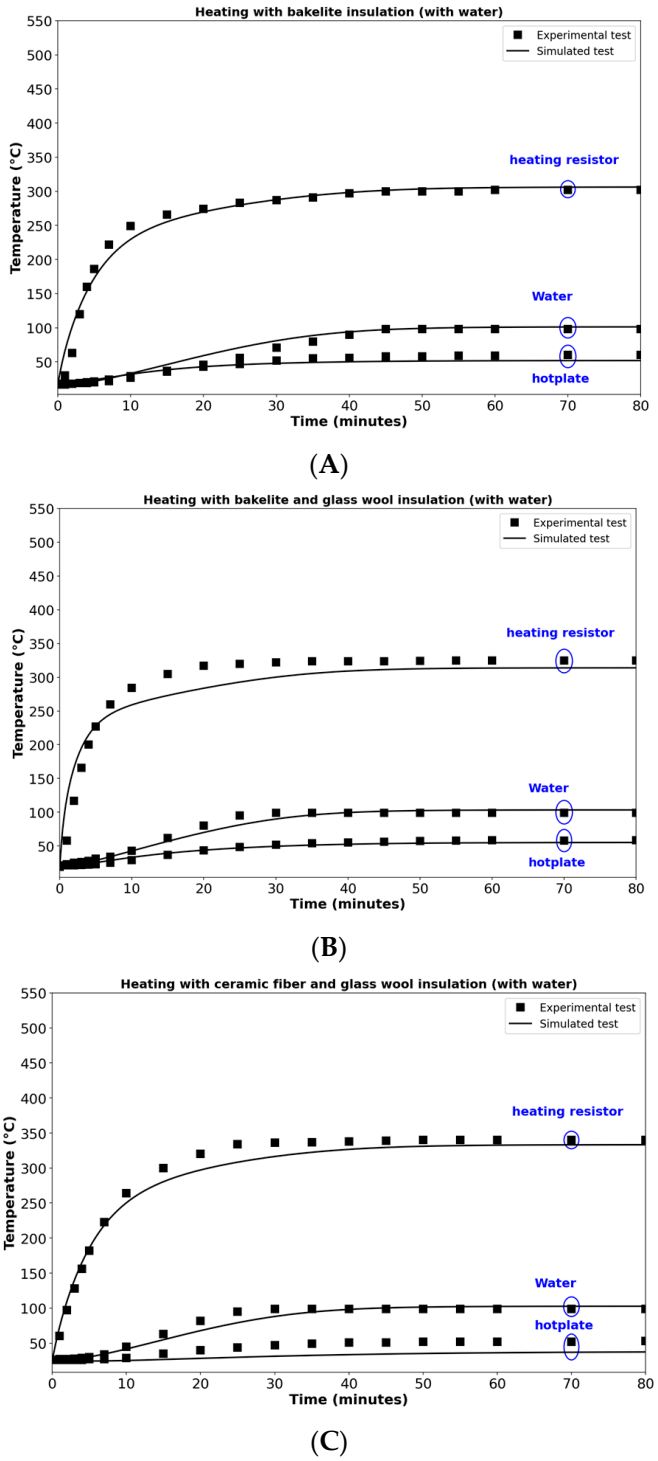

Figure 13. Temporal analysis of temperatures for different insulation configurations when heating a liter of water: simulation and experimentation. (**A**): Heating with Bakelite insulation (with water) (**B**): Heating with Bakelite and glass wool insulation (with water). (**C**): Heating with ceramic fiber and glass wool insulation (with water).

All the results obtained for the heating of a liter of water show a very good agreement between the numerical simulations and the experimental data, with differences of less than 5%, thus confirming the robustness of the theoretical model. The correlation observed for all the experimental scenarios (with or without insulation) attests to the model's ability to correctly predict the thermal behavior of the cooker in the cooking regime. The maximum temperature of the heating element is around 345 °C for the ceramic fiber and glass wool

configuration, compared to 240 °C without insulation. This improvement of nearly 44% is attributed to the effective containment of heat around the resistor. Indeed, the ceramic fiber, thanks to its low thermal conductivity (~0.08 $W \cdot m^{-1} \cdot K^{-1}$) and its high thermal resistance (up to 1200 °C), limits conduction losses and maintains a temperature gradient favorable to heat transmission to the hob. Glass wool complements this role by reducing convection losses to the base of the system.

This optimized configuration also results in a significant reduction in boiling time, from 48 min without insulation to 23 min with ceramic insulation—a 52% gain. This result clearly illustrates the impact of thermal insulation on the overall energy performance of the cooker.

In conclusion, the results demonstrate that the proposed photovoltaic solar cooker has superior heating performance than that reported in the literature, validating the heat transfer model and highlighting the relevance of the ceramic fiber + glass wool configuration for energy-efficient solar cooking applications.

5.4. Cooking Experimentation

After the thermal validation of the solar photovoltaic cooker with vacuum and load (water heating), it is necessary to evaluate its behavior under real cooking conditions. This step makes it possible to verify the system's ability to provide sufficient and stable heat for different types of food, and to measure the effectiveness of insulation and thermal regulation in practical situations. Experiments were carried out on representative dishes of the domestic kitchen, by powering the cooker either directly from the photovoltaic panels or via storage in the batteries.

Table 2 shows the experimental results of heating water and cooking different types of dishes using the solar cooker shown in Figure 7, which is powered either directly by photovoltaic panels or by batteries. During our experiments, we recorded the input and output electrical powers and the efficiencies of converters 1 and 2 (Pe, Ps, η1, η2), the temperature of resistors 1 and 2 (Tr), the temperature of the sheet plate (Tt), the cooking temperature of the food (Tc), and the cooking time (Tcoc). Regarding battery power, we have also determined and represented, in the same table, the capacity of the battery used (Cbat) as well as the discharge percentage. The results obtained show:

- When powered by photovoltaic panels, the input and output electrical powers of converter 1 vary between 319 and 335 W, and 284 and 320 W, respectively. The thermal efficiencies of this converter (η1) are very high, ranging from 84% to 97%, which attests to the proper functioning of the power block. The final temperature of the water and food reaches 100–114 °C depending on the type of cooking, allowing the boiling of water as well as the cooking of eggs, rice, tagine, fries, and bread. The cooking time varies from 20 to 45 min, or longer for large dishes such as tagine (2 kg).
- When powered by batteries, the input and output electrical powers of converter 2 vary between 340 and 347 W, and 325 and 328 W, respectively. The thermal efficiencies of this converter (η2) remain very high, between 92% and 95%, which confirms the proper functioning of the power block. The final temperature of the food reaches 100–122 °C depending on the type of cooking, allowing the boiling of water as well as the cooking of eggs, rice, tagine, fries, and bread. Cooking time ranges from 20 to 53 min, slightly reduced for some dishes compared to direct panel feeding. The capacity of the batteries used is between 1.44 and 5.4 Ah, and the discharge percentage remains very low (<1% for most dishes), indicating efficient energy management and high autonomy.

Table 2. Heating water and cooking daily meals with the cooker shown in Figure 7, powered by photovoltaic panels and batteries.

Power Mode	Photovoltaic Panels							Batteries								
Characteristics / Place	Pe (W)	Ps (W)	η_1 (%)	Tr (°C)	Tt (°)	Tc (°C)	Tcoc (mn)	Pe (W)	Ps (W)	η_2 (%)	Tr (°C)	Tt (°C)	Tc (°C)	Tcoc (mn)	Cbat Ah	Discharge (%)
Boiling water (1 L) 	327	310	94	464	55	100	20	340	325	95	400	53	100	21	2.4	1
Preparing tea and cooking 3 eggs 	320	286	89	374	51	100	23 2	347	328	94	291	61	100	20 2	2.4 0.24	1
Cooking rice (200 g) 	329	320	97	185	55	100	36	344	327	95	259	53	100	40	2.4	2
Preparation of a tagine (2 Kg) 	324	313	96	287	57	100	58	345	323	93	232	61	100	53	5.4	<3
Cooking fries (400 g) 	319	311	97	341	55	114	35	344	325	94	266	66	122	30	2.4	1.5
Bread preparation 	335	284	84	376	88	107	55	345	318	92	307	86	101	50	1.44	<3

Comparing the two power modes shows that the solar cooker works efficiently in both configurations, with some notable differences:

- Electrical powers and efficiency: Battery power has slightly higher input and output powers (Pe: 340–347 W, Ps: 325–328 W) compared to direct PV panel power (Pe: 319–335 W, Ps: 284–320 W). Thermal efficiencies remain very high in both cases, slightly higher for panel power (η1: 84–97%) compared to batteries (η2: 92–95%), indicating that both power blocks are functioning well.
- Final temperatures: The temperatures reached are comparable for the two modes, varying from 100 to 114 °C for the panels and from 100 to 122 °C for the batteries, allowing the boiling of the water and the cooking of the different dishes tested. Battery power sometimes reaches slightly higher temperatures, providing a slight advantage for some dishes.
- Cook time: Cook times are similar, ranging from 20 to (58) minutes for panels and 20 to 53 min for batteries. Bulky dishes, such as tagine (2 kg), require more time in both modes, but battery power sometimes shows a slight reduction in cooking time for some dishes.
- Autonomy and energy management: Battery power is particularly advantageous in terms of flexibility and energy management, with capacities between 1.44 and 5.4 Ah

and a very low discharge percentage (<1% for most dishes). This ensures a high level of autonomy and guarantees cooking even in the absence of direct sunlight.

All the results obtained with our solar cooker, whether powered directly by photovoltaic panels or by batteries, show higher performance and cooking times than those reported in the literature for thermal [32], parabolic [33], or electric cookers using PV panels or batteries [34] without control systems. Significant improvements have been observed, reasonable for heating temperature and cooking time. In addition, compared to conventional gas cooking [35] or electricity [36], our solar cooker has several advantages: it allows you to reach adequate temperatures for boiling and cooking various dishes, while significantly reducing fossil energy consumption. Generally, cooking temperatures are observed to be 15–25% higher, and cooking times are reduced for similar dishes [18–20,32,33].

Cooking times are slightly longer for some large dishes, but are still compatible with everyday household use. In addition, battery power provides flexibility and autonomy, allowing cooking even in the absence of direct solar radiation, which is a major advantage over conventional solar cookers and makes the system competitive with traditional methods. The combination of optimized insulation, battery storage, and thermal regulation results in high temperatures, reasonable cooking times, and sufficient runtime for everyday use, even in the absence of direct sunlight. The prototype is therefore ready for efficient and energy-efficient domestic applications.

5.5. Analysis of the Cooker Efficiency

The thermal efficiency of the cooker was evaluated under different insulation configurations while maintaining a constant Total Input Power of 350 W. This analysis is based on the experimental tests presented in Section 5.3, where 1 L of water was heated under various insulation conditions. The evaluation relies on the Useful Power effectively transferred to the water and on the thermal efficiency, defined using the following relationships:

$$\eta = \frac{P_{useful}}{P_{in}}$$

$$\eta = \frac{Q_{useful}}{P_{in} \,.\, t}$$

The useful heat is calculated as:

$$Q_{useful} = m_w \cdot C_{p,w} \cdot (T_b - T_i)$$

where

- η = thermal efficiency
- P_{useful} = useful power transferred to the water (W)
- P_{in} = electrical input power supplied to the cooker (350 W)
- Q_{useful} = useful heat gained by the water (J)
- t = heating duration (s)
- m_w = mass of water (1 kg)
- $C_{p,w}$ = specific heat capacity of water ($J \cdot kg^{-1} \cdot K^{-1}$)
- T_b = final water temperature (°C)
- T_i = initial water temperature (°C)

These relationships provide the basis for calculating the thermal efficiency of each insulation prototype:

- Heating without insulation: In the absence of insulation, only ≈120.46 W of Useful Power contribute to heating the water. The resulting thermal efficiency is 34.4%,

indicating that most of the supplied energy is not converted into useful heating. This configuration highlights the strong sensitivity of the system to thermal losses when the walls are not insulated, leading to longer heating times and a significant reduction in operational autonomy.

- Heating with insulation:
  - ✓ First configuration: Bakelite alone. The addition of Bakelite disks increases the Useful Power to ≈152.2 W, representing a noticeable improvement compared with the non-insulated case. The thermal efficiency reaches 43.5%, and the heating time is reduced by 10 min, indicating a better concentration of heat flow toward the water. However, a considerable portion of the supplied energy is still not converted into useful heat, showing that Bakelite alone remains insufficient to effectively limit lateral and upward heat losses.
  - ✓ Second configuration: Bakelite + glass wool. The combined use of Bakelite and glass wool results in a significant increase in Useful Power, reducing the heating time for 1 kg of water from 38 min to 27 min. The thermal efficiency reaches 58.2%, indicating that more than half of the supplied energy is now converted into useful heat. This configuration demonstrates the relevance of multilayer insulation for improving vertical heat transfer while minimizing lateral thermal losses.
  - ✓ Third configuration: ceramic fiber + glass wool. The configuration combining ceramic fiber and glass wool provides the best thermal performance. The Useful Power becomes sufficiently high to reduce the heating time to 23 min, and the thermal efficiency reaches 64%. This configuration therefore represents the optimal solution, ensuring maximum energy transfer to the water while maintaining excellent thermal stability and structural durability of the cooker.

This superior performance can be attributed to:

- The very low thermal conductivity of ceramic fiber;
- Its high resistance to prolonged high temperatures;
- The durability and stability of the multilayer insulation.

To assess the contribution of this study, it is essential to compare the thermal efficiency achieved by the proposed cooker with that of the reference solar and electric cooking systems reported in the literature. Box-type solar cookers, which directly convert incident solar radiation into heat at the absorber and the cooking vessel, typically exhibit thermal efficiencies ranging from ≈10% to 40% for conventional designs, depending on climatic conditions and the quality of thermal insulation [37,38]. Recent improvements, such as the integration of finned cooking pots and the use of advanced insulating materials, have significantly enhanced these performances. For instance, Vengadesan and Senthil reported a maximum thermal efficiency of approximately 56% for a box-type solar cooker equipped with a finned vessel and tested under outdoor conditions [14]. This value currently represents the upper performance limit for optimized box-type solar cookers.

Electric solar cookers, on the other hand, rely on a two-step energy conversion process: solar radiation is first converted into electricity using photovoltaic panels, and then into heat within an electric cooking device (heating element, pressure cooker, etc.). Experimental tests conducted on direct-current photovoltaic cookers have reported water-heating efficiencies between 42% and 49%, depending on solar conditions and the type of cooking vessel used [39]. Moreover, Water Boiling Tests performed on several solar electric pressure cookers have shown average thermal efficiencies exceeding 60%, corresponding to Tier 4 performance as defined by the Global Alliance for Clean Cookstoves [40].

In this context, the experimental thermal efficiencies obtained for our autonomous photovoltaic cooker—58.2% for the Bakelite + glass wool configuration and up to 64% for the ceramic fiber + glass wool configuration—fall within the upper range of values reported for optimized thermal box-type solar cookers (≈60–64%) as well as for the most efficient solar electric pressure cookers (>60%).

These results demonstrate that, despite its relatively modest electrical input power (350 W) and its hybrid PV/battery operating architecture, the proposed cooker achieves a thermal efficiency level comparable to, or even exceeding, that of the most advanced solar cooking systems available in the literature. Most importantly, it offers the major advantage of providing continuous operation, both day and night, thus ensuring a level of usability and flexibility that surpasses conventional box-type solar cookers, which remain limited by the intermittency of solar irradiation.

5.6. Techno-Economic Study of the Cooker

The Initial Investment Cost (CAPEX) of our solar cooker system (detailed in Table 3) was calculated by aggregating the costs of all components across the four major functional blocks. This breakdown serves as the basis for assessing the system's long-term economic viability. The total CAPEX for the prototype amounts to USD 1141.2. This distribution highlights the emphasis placed on autonomy and energy storage:

- Energy Production and Storage (USD 884, i.e., 77.4% of total CAPEX): This block constitutes the majority of the initial investment, primarily attributable to the PV panels (4 × 300 Wp) and, crucially, the battery system (4 × 12 V/250 Ah). This storage is essential to guarantee an autonomy of 6 to 10 days and allow continuous cooking even in the absence of direct solar radiation.
- Cooking Unit (USD 116.5, i.e., 10.2% of total CAPEX): This block, comprising the heating plate, resistors, and optimized insulation (ceramic fiber, glass wool, and Bakelite), represents a modest share of the overall cost, reflecting an effective material choice for the thermal core.
- Electronic Management and Control (USD 133.9, i.e., 11.7% of total CAPEX): This block covers the system's advanced features, including DC/DC converters and the microcontroller for intelligent energy management (MPPT, automated switching). This cost is justified by the requirement for an autonomous, flexible system, ensuring high-efficiency energy transfer and precise control.
- Miscellaneous and Tooling (USD 6.8, i.e., 0.6% of total CAPEX): This minor contribution covers the standard hardware necessary for the final assembly of the system.

This analysis confirms that the primary initial economic barrier is linked to energy storage. Consequently, the long-term economic justification of the system must focus on its performance over its lifespan and the subsequent reduction in operational expenditure (OPEX) compared to conventional cooking methods. To demonstrate the competitiveness and long-term viability of our solution, a Return on Investment (ROI) analysis was conducted by factoring in the operational expenditure (OPEX). We established that the system provides an estimated gross annual saving of USD 300 by replacing conventional fuel usage. A major technical advantage of our design is the extended battery lifespan, estimated between 8 and 10 years, which significantly reduces maintenance costs. By amortizing the cost of battery replacement over an average of 9 years, the annual operational expenditure is minimized. The household's net annual saving thus amounts to USD 264.44. To evaluate the economic performance, the Return on Investment (ROI) is calculated as a

function of the initial investment cost (CAPEX) and the net annual saving (S_{net}) using the following equation:

$$ROI = \frac{CAPEX}{S_{net}}$$

Table 3. Average cost of our cooker equipment (Figure 1).

Functional Block	Key Components and Specifications	Quantity	Total Cost (USD)
1. Energy Production and Storage	• PV Panels (1200 Wp): 4 × 300 Wp • Batteries (12 kWh): 4 × 12 V/250 Ah • Charge Controller (60/80 A) • Others (Cables, Fuses, Breakers)	4 4 1 -	720 80 80 4
	Sub-Total Block 1		884
2. Cooking Unit	• Heating Plate + Resistors (2 × 18 Ω) • Insulation (Bakelite, Ceramic Fiber, Glass Wool)	1 -	115 1.5
	Sub-Total Block 2		116.5
3. Electronic Management and Control	DC/DC Converters, Microcontroller (Raspberry Pi Pico W), Sensors, Display, Enclosure, User Interface.	-	133.9
4. Miscellaneous and Tooling	Electrical hardware and connectors	-	6.8
TOTAL INITIAL INVESTMENT COST (CAPEX)	Sum of Blocks 1 to 4		1141.2

Applying the *ROI* formula, we achieve a Return on Investment of only 4.31 years. This result is highly favorable: with a photovoltaic panel lifespan of 25 years, the system allows users to realize substantial savings for more than two decades after the initial amortization. This analysis confirms that our solar cooker is a technologically advanced, autonomous, and, critically, highly competitive economically, offering strong profitability for rural households.

To clearly position our solution in the sustainable cooking technology market, a comparative analysis of performance and costs was conducted against the main alternatives: concentrating solar thermal cookers [12,14] and conventional gas stoves. Table 4 summarizes this comparison. The analysis demonstrates that our smart PV cooker offers the best combination of technical performance and operational flexibility:

- Technical Performance (Speed): Unlike the parabolic cooker, our system achieves cooking and boiling times (less than 20–23 min for 1 L of water) that match the speed of gas stoves. This resolves the primary obstacle to the adoption of solar solutions: excessive cooking time.
- Operational Flexibility: The integration of storage eliminates the fundamental weakness of other solutions: dependence. The gas cooker relies on a costly and polluting

fuel supply; the thermal cooker is cumbersome and depends on the exact time and constant orientation of the sun. Our solution is Continuous (Day and Night) and requires no manual orientation, ensuring essential autonomy.

- Long-Term Economic Competitiveness: Although the initial CAPEX (USD 1141.2) is higher, this cost represents added value (storage and control). The rapid Return on Investment (ROI) of 4.31 years proves that the initial investment translates into the best long-term profitability, surpassing the low initial costs of other options that offer neither the necessary performance nor flexibility.

Table 4. Comparative analysis of technical performance and economic criteria between the proposed smart PV cooker and conventional alternatives.

Criterion	Photovoltaic Cooker (This Work)	Concentrating Solar Thermal Cooker (Parabolic) [12,14]	Gas Stove (Conventional)
Average Cooking Time	<45–50 min	>1 h	<45–50 min
Boiling Time (1 L water)	<20–23 min	>35 min	15–20 min
Initial Investment Cost (CAPEX)	USD 1141.2	USD 150–200	USD ~500 (average stove)
Flexibility/Autonomy	• Continuous (day and night), • No orientation required.	• Intermittent (day only), • Constant orientation required. Cumbersome.	Continuous (subject to gas supply)
Verdict	Best performance/flexibility/long-term profitability compromise	Low initial cost, limited performance and flexibility.	High operational cost, dependence on fossil fuels

In conclusion, our Smart PV Cooker is positioned as the solution that fully meets modern requirements for performance, reliability, and economic and environmental sustainability.

6. Conclusions

The work presented in this paper deals with the design, modeling, and experimental validation of an innovative, intelligent, and autonomous photovoltaic solar cooker, integrating a robust battery storage system. The device combines a 1200 W photovoltaic source, a control box equipped with DC/DC converters and a microcontroller for intelligent energy management, and a thermally insulated heating plate with two resistors. The analysis of the results obtained shows:

- ✓ The experimental results confirm the relevance of the thermal model developed, with an excellent agreement between simulations and measurements (difference <5%).
- ✓ The optimization of the insulation, combining ceramic fiber and glass wool, has made it possible to significantly reduce heat losses and to reach firing temperatures of 100 to 122 °C depending on the type of dish. Cooking times range from 20 to 45 min for most domestic dishes and up to 58 min for the 2 kg tagine. This optimal configuration achieved a high thermal efficiency of 64%.
- ✓ Intelligent energy management and battery storage allow the cooker to run continuously for 6–10 days, even in the absence of direct solar radiation. The power blocks achieve an efficiency of 95%, contributing to the overall efficiency of the system.
- ✓ Techno-Economic Analysis: Although the Initial Investment Cost (CAPEX of USD 1141.2) is higher due to the integrated storage system, the system demonstrates strong long-term economic competitiveness. With an estimated annual net saving of USD 264.44, the system achieves a highly favorable Return on Investment (ROI) of only 4.31 years, allowing substantial savings over the PV panel lifespan.

Compared to conventional gas, wood, or existing solar cooker solutions, this system stands out for its superior energy performance, flexibility of use, safety, and simplicity of operation, while reducing environmental impact. The experimental results also show that the cooker outperforms the performance reported in the literature, with cooking temperatures 15–25% higher and reduced cooking times for similar dishes, while offering unmatched autonomy [18–20,32,33].

Thus, the solar cooker developed is a sustainable, energy-efficient, and high-performance domestic solution, capable of efficiently cooking a wide range of dishes. It offers autonomy, reliability, and comfort of use, and, critically, demonstrates rapid profitability, representing an innovative alternative to traditional cooking systems.

Author Contributions: Conceptualization, S.C., O.D. and K.K.; Methodology, O.D.; Software, B.Z. and M.H.; Validation, B.Z., M.H., A.E.A. and R.M.; Formal Analysis, A.E.A.; Investigation, K.K.; Data Curation, S.C.; Writing—Original Draft Preparation, M.H.; Writing—Review and Editing, N.B.; Visualization, R.M.; Project Administration, O.D. and K.K.; All authors have read and agreed to the published version of the manuscript.

Funding: This research was funded by the Morocco-Wallonie Brussels Cooperation Program (2023–2027), Wallonie-Bruxelles-International (Belgium), Project WBI 3.3, and by the Solar Indoor Cooking Systems of the Next Generation (SoCoNexGen) project (2022–2025), part of the Europe-Africa Long-term Partnership on Renewable Energy (LEAP-RE), with funding provided by the Minister of Higher Education, Scientific Research and Innovation, Morocco, under Grant Agreement 963530 of the European Union's Horizon 2020 Research and Innovation Program. The APC was waived. All funding information has been checked for accuracy.

Data Availability Statement: The original contributions presented in this study are included in the article. Further inquiries can be directed to the corresponding author.

Conflicts of Interest: The authors declare no conflict of interest.

Appendix A

Table A1. Fundamental Parameters Used for Thermal Modeling and Simulations.

Properties	Symbol	Formula
Thermal expansion coefficient	β_v	$\frac{1}{(T_{v,i}+273)}$
Specific heat capacity of Bakelite	$C_{p,B}(T_B)$	$1250 + 0.05 \cdot T_B$
Specific heat capacity of the ceramic fiber	$C_{p,CF}(T_{CF})$	$1000 + 0.1 \cdot T_{CF}$
Specific heat capacity of iron	$C_{p,Fe}(T_{Fe})$	$440 + 0.2 \cdot T_{Fe}$
Specific heat capacity of silicone	$C_{p,Ga}(T_{Ga})$	$1460 + 0.08 \cdot T_{Ga}$
Specific heat capacity of glass wool	$C_{p,GW}(T_{GW})$	$800 + 0.05 \cdot T_{GW}$
Specific heat capacity of stainless steel	$C_{p,SS}(T_{SS})$	$450 + 0.1 \cdot T_{SS}$
Specific heat capacity of the steel	$C_{p,Sup}(T_{Sup})$	$496 + 0.2 \cdot T_{Sup}$
Specific heat capacity of the fluid	C_v	$999.2 + 0.1434 \cdot T_{v,i} + 1.101 \cdot 10^{-4} \cdot T_{v,i}^2 - 6.7581 \cdot 10^{-8} \cdot T_{v,i}^3$

Table A1. *Cont.*

Properties	Symbol	Formula
Effective emissivity	ε_{eff} [26,29]	$\frac{1}{\left[\frac{1}{\varepsilon_{Water}}+\frac{1}{\varepsilon_{G}}-1\right]}$
Modified Grashof number	Gr' [27]	$\frac{\beta.g.{d_v}^3.\mathrm{p}^2.\Delta T}{\mu^2}$
	h_{cv} [29]	$\frac{(Nu)_i\lambda_i}{d_{v,i}}$
Thermal conductivity of the Bakelite	$\lambda_B(T_B)$	$0.22+0.0001\cdot T_B$
Thermal conductivity of ceramic fiber	$\lambda_{CF}(T_{CF})$	$0.06+0.0001\cdot T_{CF}$
Thermal conductivity of iron	$\lambda_{Fe}(T_{Fe})$	$70-0.02\cdot T_{Fe}$
Thermal conductivity of the silicone seal	$\lambda_{Ga}(T_{Ga})$	$0.2+0.0002\cdot T_{Ga}$
Thermal conductivity of glass wool	$\lambda_{GW}(T_{GW})$	$0.035+0.00004\cdot T_{GW}$
Thermal conductivity of stainless steel	$\lambda_{SS}(T_{SS})$	$14+0.015\cdot T_{SS}$
Thermal conductivity of the steel support	$\lambda_{Sup}(T_{Sup})$	$51-0.05\cdot T_{Sup}$
Thermal conductivity	λ_v	$0.0244+0.7673\cdot10^{-4}\cdot T_{v,i}$
Viscosity	μ_v	$1.718\cdot10^{-5}+4.62\cdot10^{-8}\cdot T_{v,i}$
Nusselt number	$(Nu)_i$	$C.(Ra)^n$
Effective sky temperature	$\mathrm{T_c}$ [29]	$0.00552.(\mathrm{T_{amb}})\ 3/2$
Average steam temperature	T_v	$\frac{(T_{Water}+T_{cond})}{2}$
Prandtl number	Pr	$\frac{\mu.c}{\lambda}$
Partial saturated vapor pressure at water temperature	P_{Water} [29]	$exp\left[25.317-\frac{5144}{(T_v+273)}\right]$
Rayleigh number	Ra	$Gr'.Pr$
Density	ρ_v	$\frac{353.44}{(T_v+273.15)}$

References

1. Perera, F. Pollution from Fossil-Fuel Combustion is the Leading Environmental Threat to Global Pediatric Health and Equity: Solutions Exist. *Int. J. Environ. Res. Public Health* **2018**, *15*, 16. [CrossRef]
2. Wang, H.; Wang, Y. Estimating per Capita Primary Energy Consumption Using a Novel Fractional Gray Bernoulli Model. *Sustainability* **2022**, *14*, 2431. [CrossRef]
3. Safarian, S. Climate Impact Comparison of Biomass Combustion and Pyrolysis with Different Applications for Biochar Based on LCA. *Energies* **2023**, *16*, 5541. [CrossRef]
4. Paris, E.; Carnevale, M.; Palma, A.; Vincenti, B.; Salerno, M.; Proto, A.R.; Papandrea, S.; Guerriero, E.; Perilli, M.; Cerasa, M.; et al. Biomass Combustion in Boiler: Environmental Monitoring of Sugar Markers and Pollutants. *Atmosphere* **2024**, *15*, 427. [CrossRef]
5. Elfaki, K.E.; Heriqbaldi, U. Analyzing the Moderating Role of Industrialization on the Environmental Kuznets Curve (EKC) in Indonesia: What Are the Contributions of Financial Development, Energy Consumption, and Economic Growth? *Sustainability* **2023**, *15*, 4270. [CrossRef]
6. FAO. 2.5 Wood Energy and Non-Wood Forest Products Play Major Roles in the Majority of Rural Households. Available online: https://www.fao.org/3/cb9360en/online/src/html/wood-products-energy-households.html (accessed on 10 November 2025).
7. Oluwole, T.S.; Adesiyan, A.T.; Ojo, T.O.; Elhindi, K.M. Drivers of Rural Households' Choices and Intensity of Sustainable Energy Sources for Cooking and Lighting in Ondo State, Nigeria. *Sustainability* **2024**, *16*, 4556. [CrossRef]
8. Full Article: Rural Households' Behaviour Towards Modern Energy Technology Adoption Choices in East Gojjam Zone of Ethiopia: A Multivariate Probit Regression Analysis. [En Ligne]. Available online: https://www.tandfonline.com/doi/full/10.1080/23311916.2023.2178107?utm_source=chatgpt.com (accessed on 10 November 2025).
9. Apte, K.; Salvi, S. Household air pollution and its effects on health. *F1000Research* **2016**, *5*, 2593. [CrossRef] [PubMed]

10. Mawire, A.; Lentswe, K.; Owusu, P. Performance of two solar cooking storage pots using parabolic dish solar concentrators during solar and storage cooking periods with different heating loads. *Results Eng.* **2022**, *13*, 100336. [CrossRef]
11. Gorjian, A.; Rahmati, E.; Gorjian, S.; Anand, A.; Jathar, L.D. A comprehensive study of research and development in concentrating solar cookers (CSCs): Design considerations, recent advancements, and economics. *Sol. Energy* **2022**, *245*, 80–107. [CrossRef]
12. El Moussaoui, N.; Talbi, S.; Atmane, I.; Kassmi, K.; Schwarzer, K.; Chayeb, H.; Bachiri, N. Feasibility of a new design of a Parabolic Trough Solar Thermal Cooker (PSTC). *Sol. Energy* **2020**, *201*, 866–871. [CrossRef]
13. Verma, S.; Banerjee, S.; Das, R. A fully analytical model of a box solar cooker with sensible thermal storage. *Sol. Energy* **2022**, *233*, 531–542. [CrossRef]
14. Vengadesan, E.; Senthil, R. Experimental investigation of the thermal performance of a box type solar cooker using a finned cooking vessel. *Renew. Energy* **2021**, *171*, 431–446. [CrossRef]
15. Jassim, M.M.; Abbood, M.H.; Rashid, F.L. Design and Construction Solar Oven Sterilizer. *Int. J. Heat Technol.* **2022**, *40*, 641–645. [CrossRef]
16. Zafar, H.A.; Badar, A.W.; Butt, F.S.; Khan, M.Y.; Siddiqui, M.S. Numerical modeling and parametric study of an innovative solar oven. *Sol. Energy* **2019**, *187*, 411–426. [CrossRef]
17. Getnet, M.Y.; Gunjo, D.G.; Sinha, D.K. Experimental investigation of thermal storage integrated indirect solar cooker with and without reflectors. *Results Eng.* **2023**, *18*, 101022. [CrossRef]
18. Joshi, S.; Jani, A. Design, development and testing of a small scale hybrid solar cooker. *Sol. Energy* **2015**, *122*, 148–155. [CrossRef]
19. Altouni, A.; Gorjian, S.; Banakar, A. Development and performance evaluation of a photovoltaic-powered induction cooker (PV-IC): An approach for promoting clean production in rural areas. *Clean. Eng. Technol.* **2022**, *6*, 100373. [CrossRef]
20. Lecuona-Neumann, A.; Nogueira-Goriba, J.I.; Famiglietti, A.; Rodríguez-Hidalgo, M.d.C.; Boubour, J. Solar Photovoltaic Cooker with No Electronics or Battery. *Energies* **2024**, *17*, 1192. [CrossRef]
21. Atmane, I.; El Moussaoui, N.; Kassmi, K.; Deblecker, O.; Bachiri, N. Alternating multi-stage maximum power point tracking controlled parallelled photovoltaic systems for "solar cooker". *Int. J. Circuit Theory Appl.* **2021**, *49*, 3908–3921. [CrossRef]
22. Hmich, M.; Zoukarh, B.; Malek, R.; Chadli, S.; Deblecker, O.; Kassmi, K.; Bachiri, N. Design and experimentation of an innovative photovoltaic solar cooker with battery storage: A sustainable solution for Africa's future. *Sci. Afr.* **2025**, *29*, e02791. [CrossRef]
23. Hmich, M.; Chadli, H.; Chadli, S.; Salmi, K.; Malek, R.; Deblecker, O.; Kassmi, K.; Bachiri, N. Innovative electric heating system for a hybrid solar cooker (photovoltaic/thermal) using photovoltaic energy with battery storage. *Interactions* **2024**, *245*, 329. [CrossRef]
24. A New 4th Order Hybrid Runge-Kutta Methods for Solving Initial Value Problems (IVPs), Pure and Applied Mathematics Journal, Science Publishing Group. [En Ligne]. Available online: https://www.sciencepublishinggroup.com/article/10.11648/j.pamj.20180706.11?utm_source=chatgpt.com (accessed on 1 November 2025).
25. Worou, C.N.; Kang, J.; Shen, J.; Yan, P.; Wang, W.; Gong, Y.; Chen, Z. Runge–Kutta Numerical Method Followed by Richardson's Extrapolation for Efficient Ion Rejection Reassessment of a Novel Defect-Free Synthesized Nanofiltration Membrane. *Membranes* **2021**, *11*, 130. [CrossRef]
26. Pirkandi, J.; Kassaei, F.; Hashemabadi, M. Experimental Investigation of Simultaneous Effect of Parabolic Trough Collector and Flat External Reflectors on Performance of Stepped Solar Still. *Water Supply* **2022**, *22*, 3086–3102. [CrossRef]
27. Chen, W.L.; Xie, G. Performance of Multi-Stage Tubular Solar Still Operating under Vacuum. *Renew. Energy* **2022**, *201*, 34–46. [CrossRef]
28. Kalidasa Murugavel, K.; Srithar, K. Performance Study on Basin Type Double Slope Solar Still with Different Wick Materials and Minimum Mass of Water. *Renew. Energy* **2011**, *36*, 612–620. [CrossRef]
29. Mahgoub, A.A.; Elsherbiny, S.M.; El-Masry, O.A.A.; Elsamni, O.A. Enhanced Distillate Production of Stepped Solar Still via Integration with Multi-Stage Membrane Distillation. *Sci. Rep.* **2025**, *15*, 12541. [CrossRef] [PubMed]
30. Workineh, Y.; Mekonnen, H.; Belew, B. Numerical Methods for Solving Second-Order Initial Value Problems of Ordinary Differential Equations with Euler and Runge-Kutta Fourth-Order Methods. *Front. Appl. Math. Stat.* **2024**, *10*, 1360628. [CrossRef]
31. Çengel, Y.A.; Ghajar, A.J. *Heat and Mass Transfer: Fundamentals & Applications*, 5th ed.; McGraw-Hill Education: New York, NY, USA, 2015.
32. Kumar, A.; Eswaramoorthy, M.; Kumar, R.; Goyal, R.K. A comparative analysis on concrete and granite-based heat storage materials for evening cooking stability of box-type solar cooker. *Sol. Energy* **2025**, *296*, 113577. [CrossRef]
33. Gil, R.R.; Muñoz, B.C.; González-Bravo, H.; Rodríguez, R.D. Development and experimental evaluation of a parabolic solar cooker for sustainable cooking in monsoon climates. *J. Clean. Prod.* **2025**, *523*, 146416. [CrossRef]
34. Mawire, A.; Abedigamba, O.P.; Worall, M. Experimental comparison of a DC PV cooker and a parabolic dish solar cooker under variable solar radiation conditions. *Case Stud. Therm. Eng.* **2024**, *54*, 103976. [CrossRef]
35. Datta, A.; Das, M.; Ganguly, R. Design, Development, and Technological Advancements in Gas Burners for Domestic Cook Stoves: A Review. *Trans. Indian Natl. Acad. Eng.* **2021**, *6*, 569–593. [CrossRef]

36. Plumed, E.; Lope, I.; Acero, J.; Burdio, J.M. Domestic Induction Heating System with Standard Primary Inductor for Reduced-Size and High Distance Cookware. *IEEE Trans. Ind. Appl.* **2022**, *58*, 7562–7571. [CrossRef]
37. Lahkar, P.J.; Samdarshi, S. A review of the thermal performance parameters of box type solar cookers and identification of their correlations. *Renew. Sustain. Energy Rev.* **2010**, *14*, 1615–1621. [CrossRef]
38. Abu-Khader, M.M.; Hilal, M.A.; Abdallah, S.; Badran, O. Evaluating Thermal Performance of Solar Cookers Under Jordanian Climate. *Jordan J. Mech. Ind. Eng.* **2011**, *5*, 107–112.
39. Mawire, A.; Abedigamba, O.P.; Darkwa, J.; Calautit, J.K. *Experimental Evaluation of a Solar PV DC Cooker for Rural Areas*; Social Science Research Network: Rochester, NY, USA, 2023; p. 4596186. [CrossRef]
40. Water Boiling Test Results and Discussions. Available online: https://www.enterprise.scode.co.ke/files/Water-Boiling-test-Results-and-discussions..pdf (accessed on 12 December 2025).